Travelling-wave ion mobility mass spectrometry and negative ion fragmentation of hybrid and complex *N*-glycans

David J. Harvey[1], Charlotte A. Scarff[2,3], Matthew Edgeworth[2,4], Kevin Pagel[5], Konstantinos Thalassinos[6], Weston B. Struwe[1], Max Crispin[1], James H. Scrivens[2]

1) Oxford Glycobiology Institute, Department of Biochemistry, University of Oxford, South Parks Road, Oxford, OX1 3QU, UK.
2) Department of Biological Sciences, University of Warwick, Coventry, CV47AL, UK.
3) Current address, Astbury Centre for Structural Molecular Biology, School of Molecular and Cellular Biology, University of Leeds, Leeds, LS2 9JT, UK.
4) Current address, MedImmune, Sir Aaron Klug Building, Granta Park, Cambridge, CB21 6GH, UK
5) Institute of Chemistry and Biochemistry, Freie Universität Berlin, Takustrasse. 3, 14159 Berlin, Germany.
6) Institute of Structural and Molecular Biology, Department of Biological Sciences, Birkbeck College, University of London, London, WC1E 7HX, UK.

Communications:
Dr David J. Harvey,
Oxford Glycobiology Institute,
Department of Biochemistry,
South Parks Road, Oxford,
OX1 3QU, UK.
Tel. (44) (0) 1865 275750
Fax. (44) (0) 1865 275216
e-mail david.harvey@bioch.ox.ac.uk

Abstract
Nitrogen CCSs (CCSs) of hybrid and complex glycans released from the glycoproteins IgG, gp120 (from human immunodeficiency virus), ovalbumin, α1-acid glycoprotein and thyroglobulin were measured with a travelling-wave ion mobility mass spectrometer using dextran as the calibrant. The utility of this instrument for isomer separation was also investigated. Some isomers, such as $Man_3GlcNAc_3$ from chicken ovalbumin and $Man_3GlcNAc_3Fuc_1$ from thyroglobulin could be partially resolved and identified by their negative ion fragmentation spectra obtained by collision-induced decomposition (CID). Several other larger glycans, however, although existing as isomers, produced only asymmetric rather than separated arrival time distributions (ATDs). Nevertheless, in these cases, isomers could often be detected by plotting extracted fragment ATDs of diagnostic fragment ions from the negative ion CID spectra obtained in the transfer cell of the Waters Synapt mass spectrometer. Coincidence in the drift times of all fragment ions with an asymmetric ATD profile in this work and in the related earlier paper on high-mannose glycans, usually suggested that separations were due to conformers or anomers, whereas symmetrical ATDs of fragments showing differences in drift times indicated isomer separation. Although some significant differences in CCSs were found for the smaller isomeric glycans, the differences found for the larger compounds were usually too small to be analytically useful. Possible correlations between CCSs and structural types were also investigated and it was found that complex glycans tended to have slightly smaller CCSs than high-mannose glycans of comparable molecular weight. In addition, biantennary glycans containing a core fucose and/or a bisecting GlcNAc residue fell on different mobility-*m/z* trend lines to those glycans not so substituted with both of these substituents contributing to larger CCSs.

Keywords
T-wave ion mobility; *N*-linked carbohydrates; isomers; hybrid *N*-glycans; complex *N*-glycans, negative ion, CID.

Introduction

N-glycans are those glycans attached to asparagine residues in glycoproteins when these residues are in an Asn-Xxx-Ser(Thr) motif where Xxx is any amino acid except proline. Structural analysis of these glycans typically involves their release from glycoproteins by chemical or enzymatic methods and can result in very complex mixtures as shown in Figure 1. Over one hundred individual species have been recorded in some cases[1]. Subsequent analysis is usually by mass spectrometry or HPLC[2-6]. In the first of this two-part series on high-mannose *N*-glycans[7], it was shown that the use of ion mobility adds another dimension to such mass spectrometric analyses particularly when combined with negative ion collision-induced dissociation (CID) and in this paper, we extend the methods to the structural analysis of hybrid and complex *N*-glycans with particular reference to the use of these techniques to separate isomers. The ability of any analytical technique to be able to identify isomeric compounds in complex mixtures is of particular importance in analyses of this type because many of the *N*-glycans released from glycoproteins are isomeric.

Biosynthesis of *N*-glycans involves attachment of a glycan of composition $Glc_3Man_9GlcNAc_2$ to the asparagine residues, followed by removal of the glucose residues and four of the mannose moieties to give the high-mannose *N*-glycan $Man_5GlcNAc_2$ (**1,** Scheme 1 (see Scheme 1 of the first paper in this series[7] for the structures of these compounds)). This glycan is a substrate for GlcNAc-transferase I which adds a GlcNAc residue to the 2-position of the mannose residue attached to the 3-position of the branching mannose to give **2** which then becomes the substrate for other enzymes. One pathway involves addition of galactose to the 4-position of the added GlcNAc to give **3** followed by addition of sialic acid to the 3- or 6- positions of this galactose residue. This sugar chain is known as the 3-antenna and these compounds are known as hybrid glycans. Alternatively or additionally, the two mannose residues can be removed from the mannose attached to the 6-position of the branching mannose of **2** to give **4** and **5** followed by addition of GlcNAc (**7**), galactose (**8-10**) and sialic acid to this antenna (the 6-antenn) as described above. Further enzymes add fucose to the core GlcNAc (**11**, -**16**) and additional GlcNAc-Gal-Neu5Ac antennae to either or both of the outer mannoses to give isomeric triantennary glycans such as **17** and **18** (and non-fucosylated analogues, e.g. **19** and **20**), and the tetra-antennary glycans **21** and **22**. Fucose residues can also be added to antenna, such as in structure **23**, found in α1-acid glycoprotein. GlcNAc residues (termed 'bisecting GlcNAcs') can also be added to the 4-position of the branching mannoses as in compounds **24**-**44** found in the ovalbumin (**24-36**) and the IgG (**37-44**) samples. All of these latter compounds are known as complex glycans. All of these high-mannose, hybrid and complex glycans possess the common trimannosyl-chitobiose core structure **45**, a feature that greatly assists structural identification.

From Scheme 1, which contains the structures of the glycans discussed in this paper, it can be seen that several of the glycans, particularly **5** and **6**; **8** and **9**; **10, 25, 26** and **52**; **11** and **12**; **14** and **15**; **17, 18** and **23**; **29, 30** and **40, 27** and **28**; **31** and **32; 38** and **39**; **42** and **43**; **48** and **49** are isomeric. Although mass spectrometry is capable of assigning compositions and providing branching and linkage information to the glycans, it is not a very powerful technique for discriminating between isomers unless preceded by a chromatographic inlet system. For *N*-linked glycans, at least, negative ion CID has been shown to be better than positive ion methods at detecting the presence of isomeric glycans in mixtures because of the predominance of cross-ring fragment ions that produce diagnostic mass-different ions for the isomers rather than the predominantly abundance-different glycosidic cleavage ions common to positive ion spectra[8-11]. In the previous paper on high-mannose glycans[7], ion mobility, which separates on the basis of shape as well as mass and charge, combined with negative ion CID, was shown to be capable of partial resolution of several isomers of these compounds. Several other investigators have also used ion mobility to separate isomeric carbohydrates[12-15] (and see previous paper for earlier references and the review by Gray *et al.*[16]), but only a few have examined *N*-glycans[17-20]. With reference to *N*-linked glycans, Plasencia *et al.*[20] and Jiao *et al.*[21] have proposed three structures for the glycan of composition $Hex_5HexNAc_4$ from ovalbumin and Isailovic *et al.*[22] have reported differences in the arrival time distributions (ATDs) of sialylated biantennary *N*-glycans from human serum but, in this case, specific structures were not identified.

Several of the isomers encountered in the work on high-mannose glycans showed only marginal separation, detected only by asymmetric ATDs. Nitrogen collisional cross sections (CCS)s could not, therefore, be measured directly. However, CCSs of these compounds were obtained by plotting ATDs of mass-different isomer-specific fragment ions from their negative ion CID spectra [23,24]. One of the problems encountered in the previous work[7] was the appearance of asymmetric ATDs suggesting the presence of isomers but which were later shown to be due mainly to separation of reducing-terminal anomers[25]. Such anomers, or possibly additional conformers, could be differentiated from the isomers by similarity in the asymmetric ATD profiles between the molecular and fragment ions. In this paper, we report the estimated nitrogen CCSs of several complex and hybrid glycans and use of extracted fragment ATDs to estimate the corresponding CCSs of isomers that do not produce resolved ATDs. Reduction was used to eliminate effects produced by anomers.

In addition to isomer separation, we[26,27] and other investigators[17,28-31] have found that ion mobility is an excellent technique for effectively separating glycan or glycopeptide signals from those of other materials, particularly when ions are formed in different charge states. Neutral glycans yield predominantly singly-charged glycan peaks unlike many contaminating compounds that produce multiply charged ions. Within singly charged ion band there is frequently separation between compounds of different structural type, such as glycans and polyethylene glycol (PEG)[32] and even between *N*-glycans and linear glycan polymers. Consequently, in this paper, we also examine the effect of glycan structure on the ability of ion mobility to differentiate glycans with particular structural characteristics such as the presence of core fucose or bisecting GlcNAc residues.

Materials and Methods

Materials

N-linked glycans were released with hydrazine[33,34] from the well-characterised glycoproteins porcine thyroglobulin[35,36], chicken ovalbumin[37-39] bovine fetuin[40] and α1-acid glycoprotein (AGP)[41,42] obtained from Sigma Chemical Co. Ltd., Poole, Dorset, UK. *N*-glycans from gp120 expressed in CHO cells and from immunoglobulin G (IgG) were released with protein *N*-glycosidase F (PNGase F) from within NuPAGE gels essentially as described by Küster *et al.*[26,43] and as described in the previous paper[7]. Sialylated glycans from AGP were desialylated by heating with 1% acetic acid at 80°C for 30 mins. Methanol was obtained from BDH Ltd. (Poole, UK) and ammonium phosphate was from Aldrich Chemical Co. Ltd. (Poole, UK). Dextran from *Leuconostoc mesenteroides* was obtained from Fluka (Poole, UK).

Reduction of glycans

Glycans from ovalbumin, fetuin, thyroglobulin and AGP (about 0.1 mg of each mixture) in dimethylsulfoxide (DMSO, 100 µL) were acidified to pH 3.3 with acetic acid (2 µL) and reduced with an excess of sodium cyanoborohydride (~0.1 mg, Aldrich Chemical Co. Ltd. Poole, UK) overnight. The DMSO was evaporated and the samples were cleaned as described below.

Sample preparation for mass spectrometry

Following release from the glycoproteins, all glycan samples were cleaned with a Nafion® 117 membrane as described earlier by Börnsen *et al.*[44] before examination by mass spectrometry. They were then dissolved in a solution of methanol:water (1:1, v:v) containing ammonium phosphate (0.05 M, to maximize formation of $[M+H_2PO_4]^-$ ions, the most common type of ion normally seen from biological samples). Samples were then centrifuged at 10,000 rpm (9503 x g) for 1 min to sediment any particulate matter.

Ion mobility mass spectrometers

Travelling wave ion mobility experiments were carried out in nitrogen with the original (termed G1) Waters Synapt travelling wave ion mobility mass spectrometer (TWIMS), (Waters, Manchester, UK)[45] fitted with an electrospray (ESI) ion source and with the newer Synapt G2 and G2Si instruments (Waters). Waters thin-wall nanospray capillaries and, later, gold-coated borosilicate glass capillaries[46] prepared in-house, were used for introducing the samples. Ion source conditions were: ESI capillary voltage, 1.0-1.2 kV cone voltage, 100-180 V, ion source temperature 80°C. The T-wave velocity and peak height voltages were 450 m/sec and 40 V respectively unless otherwise specified.

Fragmentation was performed after mobility separation in the transfer cell with argon as the collision gas. The Synapt G1 instrument was externally mass calibrated with sialylated *N*-glycans released from bovine fetuin, the other two instruments were mass-calibrated with dextran oligomers from *Leuconostoc mesenteroides* (negative ion measurements) or with caesium iodide (both positive and negative ion. Data acquisition and processing were carried out using the Waters DriftScope (version 2.8) software and MassLynx^{TM} (version 4.1). The scheme devised by Domon and Costello[47] was used to name the fragment ions. Additionally, ions containing the 6-antenna and core mannose residue by formal loss of the chitobiose core and 3-antenna are referred to as D ions[48].

Nitrogen CCSs were determined using dextran oligomers (Glc_2-Glc_{13}) to calibrate the travelling wave cell of the Synapt G2 and G2Si instruments. They were obtained directly on a modified Synapt quadrupole/IMS/oa-TOF MS instrument containing a linear (not travelling wave) drift tube (Waters MS-Technologies, Manchester, UK)[49-53]. CCS calibration of the G2 and G2Si instruments was performed with the method described by Thalassinos *et al.*[54] as described in the previous paper[7]. The corrected drift times of the glucose oligomers and CCSs were fitted by a power law equation of the type $Y = Ax^n$ which May *et al.*[55] have confirmed adequately fits data of this type. Projected helium CCSs were made with a helium:nitrogen cross correlation plot of CCSs of dextran recorded with the linear instrument (R^2 = 0.9989). Cross section measurements will be placed in the Glyco-Mob ion mobility database[56].

Results and Discussion

Results for high-mannose glycans reported earlier[7] showed that many isomers of these *N*-glycans could be detected by ion mobility using extracted fragment ATDs. In addition, those having the full complement of mannose residues on the 6-branch of the 6-antenna, were shown to produce relatively larger nitrogen CCSs than corresponding glycans where this mannose was missing. However, when these glycans were reduced, the ATDs from the larger glycans became more symmetrical and the difference less noticeable[25]. Asymmetry of the ATDs from higher mass high-mannose glycans was found to be due to partial resolution of anomers rather than isomers. Consequently, in the present study, glycans were also reduced to remove effects of anomer separation. CCSs of the reduced glycans were similar to but sometimes varied by several $Å^2$ in either direction from the CCS values of the unreduced glycans (Table S1).

We looked for features in both the reduced and unreduced hybrid and complex *N*-glycans that might be correlated to structure in addition to the ability of ion mobility to separate isomeric *N*-glycans. Glycans from chicken ovalbumin, thyroglobulin, IgG, AGP (desialylated) and gp120 were taken as representative examples. Negative ion mass spectra of the glycans released from these glycoproteins are shown in Figure 1.

General effects of structure on nitrogen collisional cross sections

Figure 2a shows a plot of the measured nitrogen CCSs of all major glycans from the glycan mixtures (high-mannose, hybrid and complex) against *m/z* in negative ion mode. In general, these fell roughly on the same trend line without any particular trend identifying a particular glycan type. Possible exceptions were the glycans $Hex_4GlcNAc_3$ (**8**) and $Hex_4GlcNAc_4$ (**8**, **9**) which gave slightly smaller CCSs than those falling on the general trend line. The same result was seen after reduction (Figure 2b). In positive mode (Figure 2c), the same differences were seen although they appeared to be a little more pronounced whereas, after reduction (Figure 2d), the smaller high mannose glycans (particularly $Man_5GlcNAc_2$ (**1**) and $Man_6GlcNAc_2$ (**46**) showed significantly larger CCSs.

Effect of substituents on nitrogen collisional cross sections of biantennary glycans

At a more detailed level, some trends were observed between fucosylated and bisected glycans obtained from IgG. The glycans in this glycoprotein (profile shown in Figure 1c) are biantennary complex carbohydrates with (**13-16**) and without (**7-10**) a fucose residue on the core GlcNAc and also, with a bisecting GlcNAc residue (**37-40** and **41-44**). Figure 3 shows the negative ion *m/z*:cross section plots of these compounds (phosphate adducts) measured with the Synapt G2 instrument. A parallel experiment with $[M+Cl]^-$ adducts on the G1 instrument gave identical results (not shown). The plots from the major fucosylated glycans with zero, one and two galactose residues (compounds **13-**

16, commonly known as G0F, G1F and G2F respectively) produced a linear relationship. A similar result was obtained for the corresponding compounds without fucose (**7-10**) but the plot was displaced towards shorter drift times (Figure 3). Thus, fucosylated glycans showed longer drift times and nitrogen CCSs than their unfucosylated counterparts of similar molecular weight. Similar results were obtained in positive ion mode ($[M+Na]^+$ ions) and from the G2 instrument (data not shown). When sialic acid was attached to the antennae, a similar effect was obtained; i.e. the presence of the core fucose residue produced a relative increase in the drift time of the trend line.

Corresponding plots were made with the biantennary glycans containing a "bisecting" GlcNAc residue with (compounds **41-44**) and without (**37-40**) a fucose residue. In each case, the plots were linear and the presence of the bisecting GlcNAc caused a shift to longer drift times although the effect was not as great as that for fucose. The effect of both a core-fucose residue and a bisecting GlcNAc was roughly additive (Figure 3). Again, similar results were obtained from the G1 instrument with $[M+Cl]^-$ ions. Unfortunately, the ions from the unfucosylated compounds with bisecting GlcNAc residues in the positive ion spectra of the IgG samples were not abundant enough to give reliable readings for the CCSs.

Resolution of isomers

In general, the resolution of the ion mobility cell of the Synapt instruments was not sufficient to separate many of the isomers present in these samples. However extracted fragment ATDs of diagnostic ions[23,24,57,58] allowed the components at several *m/z* values to be deconvoluted as shown in the examples below. Comparisons of CCSs measured in this way with those measured directly with the drift tube instrument validated this approach. Nitrogen and projected helium CCSs of the glycans reported in this paper are listed in Table 1. Below are examples where this technique allowed isomers to be detected.

Glycans of composition $Man_3GlcNAc_3$ and $Man_3GlcNAc_3Fuc_1$: The ability of ion mobility to separate isomers of small *N*-linked glycans was demonstrated earlier with the Waters Synapt G1 instrument using the two $Man_3GlcNAc_3$ isomers (**5, 6,** Scheme 1) from chicken ovalbumin[19] (glycan profile in Figure 1a). Although three peaks were detected in negative ion mode, only compounds **5** and **6** were identified. Later work with the G2[59] and G2Si instruments, reported here, reproduced the positive ion separation but only resolved two isomers in negative ion mode even though the resolution was higher and suggesting that, in fact, only two compounds were present. Resolution of the two isomers was almost to baseline in positive ion mode ($[M+Na]^+$ ions, *m/z* 1136) (Figure 4a) although somewhat less so in negative mode with the $[M+H_2PO_4]^-$ ions (*m/z* 1210, Figure 4b). Reduction of the glycans made no difference to the separation. Structural assignments of the isomers were made by negative ion fragmentation (Figure 4e,f). These spectra showed that the isomer with the largest cross section had a GlcNAc residue attached to the 6-antenna (**6**) as indicated by the D, D-18, $^{0,3}A_3$ and $^{0,4}A_3$ ions at *m/z* 526, 508, 454 and 424 respectively (Figure 4f). These ions contain the branching mannose residue and substituents from the 6-antenna[11]. The linkage position of the GlcNAc residue to the 6-antenna was not determined. The isomer with the smaller cross section was the 3-substituted isomer **5** as shown by the appearance of the D, D-18, $^{0,3}A_3$ and $^{0,4}A_3$ ions 162 mass units lower at *m/z* 323, 305, 292 and 262 (Figure 4e). The positive ion spectra (Figures 4c and 4d) were virtually identical to each other and differed mainly in the relative abundance of the ion at *m/z* 388 ([Gal-GlcNAc+Na]$^+$). This difference did not allow the individual isomers to be identified, clearly emphasising the advantage of using negative ion fragmentation for deducing the structures of *N*-glycans. Jiao *et al.*[21] in an MS^n study also reported the presence of isomers of the $Man_3GlcNAc_3$ glycan containing a GlcNAc residue on either antenna but their experiment did not involve ion mobility and did not allow the compounds to be separated. A third, bisected isomer reported in their paper was not detected by us using ion mobility and negative ion CID with the G2Si instrument. Although it is possible that this isomer might have been responsible for the third peak reported earlier with the G1 instrument, the reported spectrum[19] was not consistent with a bisected structure of this type. CCSs are listed in Table 1.

The fucosylated analogues of these isomeric glycans (**11**, **12**), present in the mixture of glycans released from thyroglobulin (Figure 1b) and gp120 (Figure 1d) also showed separation but the

difference in nitrogen CCSs were less, such that only a single broad ATD peak was observed. Possibly different linkage isomers were present to those being separated than for the un-fucosylated isomers discussed above, but this was not determined. However, the CID spectra did confirm substitution of the third GlcNAc residue on either antenna. As discussed below, other pairs of isomers were found that gave different estimated nitrogen CCSs and where the unfucosylated pair gave better separations than those isomers bearing a core-fucose. These isomers (**11**, **12**) were also separated as nitrate adducts from thyroglobulin (equivalent to *m/z* 1356.4 in the glycan profile of phosphate adducts shown in Figure 1b) but, in this case, the molecular ion at *m/z* 1321.5 was coincident with that from an abundant doubly charged sialylated glycopeptide giving a complicated CID spectrum (Figure 5a). This situation provided an excellent example of where ion mobility could be used to separate these compounds. The fragments from the doubly charged ion, which fell in a different mobility band (Figure 5b), were removed by selecting only the singly charged ions from the DriftScope display (Figure 5b). Then, the CID spectra were extracted from each side of the ATD peak from the *N*-glycan (Figures 5d and 5e). These spectra were characteristically different and showed that the second isomer (Figure 5e) was the one with the GlcNAc residue on the 6-antenna (**12**). The diagnostic ions for this isomer were the D, $[D\text{-}18]^-$ and $^{1,3}A_3$ ions at *m/z* 526, 508 and 454 respectively[10,11]. In the spectrum recorded from the left-hand edge of the ATD peak (smaller cross section), these ions were missing but the D and $[D\text{-}18]^-$ ions were replaced by the corresponding ions 203 mass units lower at *m/z* 323 and 305 respectively showing that the GlcNAc residue was located on the 3-antenna (**11**). Although the shape of the ATD peak (Figure 5b) did not reflect the presence of these isomers, they were detected by differences in the extracted fragment ATDs (from Figure 5d and 5e) which maximized at different positions within the width of the ATD peak (Figure 5c), confirming the presence of isomers (indicated by the two dotted lines in Figure 5c). As with the related unfucosylated glycan from ovalbumin (**5**, **6**), the positive ion spectra for the two isomers showed little difference except for the relative abundance of the ion at *m/z* 388 and did not allow structures to be assigned to the ions.

Hybrid glycans from gp120: Other isomeric compounds that could be separated by ion mobility were the hybrid glycan pairs H_5N_3 (**2**, **47**)[27] and $H_5N_3F_1$ (**48**, **49**, positive ion)[59] reported in earlier publications. Negative ion spectra of compounds **48** and **49** are shown in Figure 6 together with that of $Hex_6GlcNAc_3Fuc_1$ (**50**, Figure 6a) released from gp120 to illustrate the general fragmentation of these hybrid glycans. $^{2,4}A_6$ and $^{2,4}A_5$ cross-ring fragment ions at *m/z* 1437 and 1234 respectively together with the B_5 fragment at *m/z* 1377 define the β1→4-linked chitobiose core and the presence of the fucose residue at the 6-position of the reducing-terminal GlcNAc. The cross-ring fragment at *m/z* 424 (Gal-GlcNAc-O-CH=CH2-O^-) is diagnostic for the galactose-terminated antenna and the composition of the 6-antenna is specified by the D, D-18, $^{0,3}A_4$, $^{0,4}A_4$ and $B_{2\alpha}$ ions at *m/z* 647, 629, 575, 545 and 503 respectively. All fragment ions show the same profile as the ATD of the molecular ion as would be expected for a single compound.

The ion at *m/z* 1680.5 in the negative ion CID spectrum of the gp120 glycans contains the two compounds (**48** and **49**). It shows an asymmetrical ATD peak attributable to these two compounds and extracted fragment ATDs clearly resolve two constituents (inset to Figure 6c). Plotting spectra from each side of the ATD peaks from these compounds (with and without fucose) allowed reasonably clean spectra of each of the constituents to be extracted (Figure 6b and 6c, with fucose and see Figure 4 from reference[27] for the compounds without fucose). Thus, the $^{2,4}A_{6(5)}$, $^{2,4}A_{5(4)}$ and $B_{5(4)}$ ions at *m/z* 1275, 1072 and 1215 respectively (Figure 6), which have the same asymmetric profile as the molecular ions, define the same core and fucose location in both compounds **48** and **49**. The first constituent (**48**, Figure 6b) produced the $^{1,3}A_3$ cross-ring fragment at *m/z* 424 confirming the Gal-GlcNAc antenna and a shift of the D, D-18, $^{0,3}A_3$, $^{0,4}A_3$ and $B_{2\alpha}$ ions to *m/z* 485, 467, 413, 383 and 341 respectively reflecting the absence of one mannose residue from the 6-antenna. The linkage position of the mannose on the 6-antenna was not determined. The spectrum of the second constituent (**49**, Figure 6c) exhibited D, D-18, $^{0,3}A_3$, $^{0,4}A_3$ and $B_{2\alpha}$ ions at the same mass as in the spectrum of compound **1** reflecting the extra mannose in the 6-antenna. Positive ion spectra of these two glycans, extracted from an asymmetrical ATD peak have been published[59].

Nitrogen CCSs were calculated from these fragment ions using extract fragment ATDs (G2Si instrument) by the method described by Thalassinos *et al.*[54] (Table 1). As was found in the earlier study on high-mannose glycans, drift times extracted from ions in the full mass spectrum were slightly higher than those measured from the same ion when selected for fragmentation and, consequently, an offset, calculated from the difference in drift times of the ions at *m/z* 1655 measured in the total mass spectrum and when the ion was selected for fragmentation. This method gave nitrogen CCSs of 385.4 and 405.0 A^2 for compounds **48** and **49** respectively. Compound **37** was considerably more abundant than compound **49** and its cross section was measured directly from the full spectrum. The value of 385.7 A^2 agreed very well with that measured by the fragment ion method for the first peak, thus validating the method.

The ion at *m/z* 1534.5 ($Hex_5GlcNAc_3$) in the negative ion spectrum of the gp120 glycans was produced by the corresponding compounds (**2**, **47**) without fucose. These compounds were similarly separated by ion mobility (not shown) and nitrogen CCSs of 373.9 A^2 and 357.6 A^2 respectively were measured for the two compounds by extracted fragment ATDs. Glycans with and without core fucose and with only four hexose residues ($Hex_4GlcNAc_3$ and $Hex_4GlcNAc_3Fuc_1$, *m/z* 1372.4 and 1518.5 respectively) in the spectrum of gp120 glycans appeared to lack the Gal-GlcNAc-containing species and to be represented by only the hybrid glycans (**4** and its core-fucosylated analogue **51**). The spectrum of $Man_4GlcNAc_3$ (**4**) is shown in Figure 6d.

Glycans of composition $Hex_5GlcNAc_4$ (m/z 1737.6) from ovalbumin: The glycan of composition $Hex_5GlcNAc_4$ from ovalbumin has predominantly the bisected hybrid structure **25** and is used as a reference standard because it has always been assumed to be a single compound. Its CID spectrum (Figure 7c) contained a prominent ion at *m/z* 629 formed as a fragment of the D ion (formal loss of the chitobiose core and the 3-antenna) by elimination of the bisecting GlcNAc residue. This prominent ion (*m/z* 629), in the absence of the related D ion, has been shown to be diagnostic for bisecting glycans with three mannose residues in the 6-antenna[10,11] confirming the structure of glycan **25**. However, a recent publication[20] reported three peaks in the mobility spectrum of the $[M+2Na]^{2+}$ ion from this glycan (per-methylated derivative) obtained from ovalbumin from the same commercial source. These compounds were assigned the structures **25, 26** and **52** on the basis of molecular modelling. Three compounds of this composition were also detected from ovalbumin by Saba *et al.*[60] using SymGlycan software but, in this case, isomers **10**, **25** and **52** were proposed. Relative quantities were not reported. The symmetrical ATD peak (Figure 7a) and mobility-separated fragmentation spectrum of this compound as its $[M+Na]^+$ and $[M+2Na]^{2+}$ ions recorded by us from our sample with the Synapt G2 and G2Si instruments showed little evidence of more than one compound (**25**). Also, ion profiles of most fragment ions in the negative ion spectrum ($[M+H_2PO_4]^-$ ion) from both the PNGase F- and endoH-released glycan were virtually identical. Figure 7b shows the ion profiles from the PNGase F-released glycans. It has yet to be determined if permethylation increases the ability to separate these isomers or if our sample has a different composition from the one used by Plasencia *et al.*[20].

The minor ion at *m/z* 424 ($[Gal\text{-}GlcNAc\text{-}O\text{-}CH{=}CH\text{-}O]^-$) in the spectrum shown in Figure 7c, is a $^{1,3}A$ cross-ring cleavage ion and is an abundant (frequently the base peak) diagnostic ion for glycans containing Gal-GlcNAc chains[11] as in the example above and suggests the presence of compounds **10** or **26** in trace amounts. The ion at *m/z* 466 (Gal-GlcNAc + 101) is also characteristic of this structural feature. The ATD profile of the ion at *m/z* 424 was slightly displaced to the left (smaller cross section) compared with those of the other fragment ions (Figure 7b) suggesting that it was not from compound **26** (assuming that the same relationship exists between CCSs in positive and negative ion modes). The positive ion cross section of compound **26** reported by Plasencia *et al.* was considerably higher than that of the main compound (**25**). Figure 7d shows the spectrum extracted from the left-hand region of the ATD peak (8.9 - 9.8 msec, Figure 7a). It contained prominent ions at *m/z* 688 and 670, corresponding to the D and D-18 ions from the biantennary glycan **10**. In addition, the cross section of this glycan calculated from the fragment ions matched that of the biantennary glycan **10** (obtained from IgG and de-sialylated fetuin, Table 1); Figure 7a shows the ATDs of this compound (from bovine fetuin) and compound **25** (from ovalbumin) showing a similar difference in drift times. The smaller cross section of the complex biantennary glycan (**10**) compared with the

bisected hybrid glycan (**25**) is consistent with the results on general trends discussed above. Slightly better separation of these compounds has been obtained previously in positive ion mode[59].

The fragmentation spectrum of glycan **52**, reported by Plasencia *et al*, would contain a prominent E-type fragment ion at *m/z* 507. An extracted fragment ATD of this ion gave two peaks; one was coincident with the bisected compound (**25**), the other displayed a longer drift time. However, this extracted fragment ATD, although suggestive, was not enough to confirm the presence of compound **52**. Plasencia *et al*. report a cross section smaller than that of glycan **25**. In our sample, therefore, the peak at *m/z* 1737 ($Hex_5GlcNAc_4$) appears to consist mainly of the bisected glycan **25**, together with a very small amount of the biantennary glycan **10**. Definitive evidence for the presence of compounds **26** and **52** in our sample was not obtained. Reduction gave only a single ATD peak with no sign of isomer separation. Unfortunately, the recent study by Jiao *et al*.[21] on isomers from ovalbumin did not include this compound.

Glycans of composition $Hex_4GlcNAc_4$ (m/z 1575.5) from ovalbumin: Many of the other ions from ovalbumin are produced by isomers[37] but few could be separated by ion mobility with the G2 instrument. One instance where isomers were partially separated was the peak at *m/z* 1575.5 corresponding to $Hex_4GlcNAc_4$ (phosphate adduct, Figure 8). In this example, three compounds were detected. The composition corresponded mainly to the structures **8** and **9** and the presence of these compounds was confirmed by extracted fragment ATDs of the $^{1,3}A_3$, D and D-18 ions (Inset to Figure 8). The negative ion CID spectrum of this ion (Figure 8) was more complicated than that observed from reference spectra of compounds **8** and **9** (obtained from IgG), consistent with work by Jiao *et al*.[21] who reported the presence of five isomers at this mass following investigations by MS^n on permethylated samples. Da Silva *et al*.[37], on the other hand, only reported the presence of the bisected compound **24**. This latter compound should produce a D-221 ion at *m/z* 467 and this ion was present, although at a relatively low abundance. Its cross section was similar to that of the 6-Gal isomer of the biantennary glycan (**9**). Reduction gave a similarly shaped ATD peak as that shown in Figure 8a (slightly extended at the right-hand edge) consistent with the presence of isomers.

Biantennary glycans: The biantennary glycans from IgG (glycan profile in Figure 1c) with one galactose residue (**8, 9, 14, 15**) exist as isomers with the galactose residue on either antennae. The presence of these isomers can be clearly seen in the negative ion fragmentation spectrum (Figure 9c, mixed isomers) by the two sets of D and D-18 ions at *m/z* 526/508 (3-galactose isomer **14**) and at *m/z* 688/670 (6-galactose isomer **15**), consistent with the data in Figure 9 and with HPLC data, the isomer with the galactose on the 3-antenna was the more abundant. It would be expected that these isomers would show a difference in drift time and this was found to be the case for the pair **8** and **9** without fucose (as in Figure 8a). A difference of about 5 $Å^2$ was measured. Extracted fragment ATDs of the diagnostic fragments are shown in Figure 9a where it can be seen that the isomer with the galactose in the 6-antenna has the longer drift time and, hence cross-section. Its longer drift time is consistent with the result from the $Man_3GlcNAc_3$ isomers (above). However, no isomeric separation could be achieved in either the G1 or G2 instruments with the corresponding pair of isomers (**14** and **15**) with a fucose residue on the core. Figure 9b shows the relevant single fragment ion profiles. However, some limited separation was found earlier for chlorine adducts of the glycans released with the enzyme endo H and, thus, missing the terminal GlcNAc residue with its attached fucose[61].

Triantennary glycans: Two triantennary structures are commonly found in *N*-glycan mixtures. These have structures **17, 18, 19 and 20**, and are readily identified by their production of diagnostic ions[62]. The isomers with two branches on the 3-antenna (**17, 19**) gives rise to a prominent fragment at *m/z* 831 and D and D-18 ions at *m/z* 688 and 670 whereas, in the spectrum of the other isomers (**18, 20**), the ion at *m/z* 831 is missing and the D and D-18 ions shift to *m/z* 1053 and 1035 accompanied by another fragment (D-36) at *m/z* 1017. Figure 10 shows a spectrum from gp120 where both isomers occur together. Extracted fragment ATDs of these diagnostic ions (*m/z* 831 and 1035, inset to Figure 10) showed that the isomer with the 6-branched antenna has a slightly larger cross section (about 6 $Å^2$) than the other isomer but the spectra were rather too weak to obtain a reliable cross section measurement. The measurement in Table 1 for glycan **19** was from AGP (Figure 1e). The isomer of glycan **19** from AGP where the fucose resides on a GlcNAc of the 3-antenna (**23**) showed a very

slightly larger cross section (about 3 $Å^2$) than that of the core-fucosylated glycan **17**. Extracted fragment ATDs of the two sets of $^{2,4}A_6$, B_5 and $^{2,4}A_5$ (*m/z* 1843, 1783, 1640 and 1989, 1929, 1786 for compounds **17** and **23** respectively) revealed the presence of the two compounds and the structures were confirmed by the presence of ions at *m/z* 831 (from **17**), the corresponding fucosylated ion at *m/z* 977 (from **23**) together with the ion at *m/z* 670 (Gal-(Fuc)GlcNAc-CH=CH2-O^- from **23**).

Conclusions

The above examples clearly show that ion mobility mass spectrometry adds a further dimension to the analysis of *N*-linked carbohydrates by mass spectrometry. Some isomeric separation was possible in both positive and negative ion modes but appeared to be marginally better in positive ion mode with, for example, $[M+Na]^+$ ions from $Man_3GlcNAc_3$. Fragmentation, however, was considerably more informative in negative ion mode and yielded mass different ions from which the structures of the glycans and the presence of isomers could be deduced. Thus, good separation of the isomers of $Man_3GlcNAc_3$ (**5**, **6**) from chicken ovalbumin was obtained and negative ion fragmentation allowed their structures to be determined. Several of the other glycans from ovalbumin were isomeric but, although some ATD peak broadening was observed with some of them, there was no obvious isomeric separation. However, if the compounds were fragmented in the transfer cell, extracted fragment ATDs showed that, in several cases, there was some separation within the peaks allowing isomers to be detected. The differences in cross section of many of these isomers were only a few $Å^2$ and often less than the experimental error in measurements made at different times. Thus, although isomers could sometimes be detected using extracted fragment ATDs, use of their estimated nitrogen CCSs for identification purposes was sometimes marginal unless internal calibration was used. In general only isomers of the smaller complex or hybrid glycans showed significant differences in cross section and it was noted that the presence of core fucose generally decreased the ability of ion mobility to separate isomers.

Some correlations between nitrogen CCSs and structure were observed. Predominantly, substitution in the 6-antenna, as found earlier with the high-mannose glycans, usually produced larger CCSs than substitution on the 3-antenna. This effect was observed for the addition of GlcNAc to $Man_3GlcNAc_2$, for galactosylation of the unfucosylated biantennary glycans and for the isomers of triantennary glycans. Glycans carrying a bisecting GlcNAc residue tended to have larger CCSs than isomeric glycans lacking this feature.

There is always the possibility with this work that the separation observed in the mobility cell is due to conformers of a single compound rather than to isomers. Recent work from this laboratory on reduced *N*-glycans[25] has shown that the predominant factor leading to asymmetrical ATD peaks in the larger high-mannose glycans is the anomeric configuration of the reducing terminal GlcNAc residue. This phenomenon is not new; separation of anomeric mono- and oligo-saccharides by ion mobility, particularly as $[M+Na]^+$ ions from methyl glycosides, has been reported on several occasions[63-67] and it has been proposed that separations reflect the way in which the adducted cation is bound to the individual sugar[68]. Whether this effect applies to the location of the phosphate adduct in the compounds reported in this paper has yet to be determined. As noted earlier[25], asymmetric ATDs were observed from the higher high-mannose glycans leading to uncertainty in the estimated nitrogen CCSs (note the larger variation in measurements for $Man_8GlcNAc_2$ (**53**) and $Man_9GlcNAc_2$ (**54**) in Table 1, compared to those of the smaller high-mannose glycans **1**, **46**, **55**). These asymmetric ATDs, which were found to be due to reducing-terminal anomers, were rendered symmetrical by reduction. In contrast to the high-mannose glycans, little or no significant effects attributable to anomeric separations were observed with the hybrid and complex glycans. However, for compounds producing asymmetric ATDs, it would be wise to fragment the compound and check if the drift time peaks of fragments attributable to potential isomers maximise at the same point in time. Following reduction, the smaller high-mannose glycans showed larger nitrogen CCSs than complex glycans of equivalent molecular weight but with other glycans, although the reduced form generally showed larger CCSs than the unreduced glycans, no consistent correlation with structure was noted.

The ability of ion mobility to separate isomers, albeit with rather low resolution at present, will be a great asset because one of the disadvantages of mass spectrometry (without fragmentation) is its

difficulty in distinguishlng between such compounds. The ion mobility resolution obtained with the Synapt instruments does not yet match that of an HPLC column but is expected to rise with further instrumental developments. Ultimately, it might be possible to achieve adequate separations in the gas phase in milliseconds rather than the tens or hundreds of minutes required at present with LC-MS systems.

The work presented here, and by other investigators, shows that ion mobility has much to offer in glycobiology and is able to solve problems such as isomer resolution that, up to now, have required chromatographic separation. Combined with its ability to extract glycan ions from complex mixtures and, thus, eliminate some clean-up stages[26], and by the production of negative ion CID spectra, the technique provides a much more rapid and information-rich method for the structural determination of *N*-glycans than has been available up to now.

Acknowledgements
We thank Professor Raymond Dwek for his help and encouragement. This work was supported by the International AIDS Vaccine Initiative Neutralizing Antibody Center CAVD grant (Glycan characterization and Outer Domain glycoform design), the Scripps CHAVI-ID (1UM1AI100663) and by the Oxford Glycobiology Bequest.

References

[1] Behrens A-J, Vasiljevic S, Pritchard LK, Harvey DJ, Andev RS, Krumm SA, Cupo A, Struwe WB, Kumar A, Zitzmann N, Seabright GE, Kramer HB, Spencer DIR, Royle L, Burton DR, Wilson IA, Ward AB, Sanders RW, Moore JP, Doores KJ, Crispin M. Composition and antigenic effects of individual glycan sites of the trimeric HIV-1 envelope. *Cell Rep.* **2016**: In Press.

[2] Harvey DJ. Proteomic analysis of glycosylation: structural determination of *N*- and *O*-linked glycans by mass spectrometry. *Expert Rev. Proteomics* **2005**; *2*: 87-101.

[3] Harvey DJ. *Electrospray and MALDI Mass Spectrometry: Fundamentals, Instrumentation, Practicalities, and Biological Applications, 2nd Edition*: Cole RB, (ed). John Wiley and Sons Inc.: Hoboken, NJ, USA, **2010**; 723-769.

[4] Alley WR, Jr., Mann BF, Novotny MV. High-sensitivity analytical approaches for the structural characterization of glycoproteins. *Chem. Rev.* **2013**; *113*: 2668-2732.

[5] Alley WR, Jr., Novotny MV. Structural glycomic analyses at high sensitivity: A decade of progress. *Annu. Rev. Anal. Chem.* **2013**; *6*: 237-265.

[6] Harvey DJ. *The analysis of post-translational modifications using mass spectrometry*: Griffiths JR, Unwin R, (ed). Wiley, **2016**; In Press.

[7] Harvey DJ, Scarff CA, Edgeworth M, Struwe WB, Pagel K, Thalassinos K, Crispin M, Scrivens J. Travelling-wave ion mobility and negative ion fragmentation of high mannose *N*-glycans. *J. Mass Spectrom.* **2016**; *51*: 219-235.

[8] Harvey DJ. Fragmentation of negative ions from carbohydrates: Part 2, Fragmentation of high-mannose *N*-linked glycans. *J. Am. Soc. Mass Spectrom.* **2005**; *16*: 631-646.

[9] Harvey DJ. Fragmentation of negative ions from carbohydrates: Part 1; Use of nitrate and other anionic adducts for the production of negative ion electrospray spectra from *N*-linked carbohydrates. *J. Am. Soc. Mass Spectrom.* **2005**; *16*: 622-630.

[10] Harvey DJ. Fragmentation of negative ions from carbohydrates: Part 3, Fragmentation of hybrid and complex *N*-linked glycans. *J. Am. Soc. Mass Spectrom.* **2005**; *16*: 647-659.

[11] Harvey DJ, Royle L, Radcliffe CM, Rudd PM, Dwek RA. Structural and quantitative analysis of *N*-linked glycans by MALDI and negative ion nanospray mass spectrometry. *Anal. Biochem.* **2008**; *376*: 44-60.

[12] Hoffmann W, Hofmann J, Pagel K. Energy-resolved ion mobility-mass spectrometry - A concept to improve the separation of isomeric carbohydrates. *J. Am. Soc. Mass Spectrom.* **2014**; *25*: 471-479.

[13] Huang Y, Dodds ED. Discrimination of isomeric carbohydrates as the electron transfer products of group II cation adducts by ion mobility spectrometry and tandem mass spectrometry. *Anal. Chem.* **2015**; *87*: 5664-5668.

[14] Ewing MA, Glover MS, Clemmer DE. Hybrid ion mobility and mass spectrometry as a separation tool. *Journal of Chromatography A, (2016)* **2016**; *1439*: 3-25.

[15] Hinneburg H, Hofmann J, Struwe WB, Thader A, Altmann F, Silva DV, Seeberger PH, Pagel K, Kolarich D. Distinguishing *N*-acetylneuraminic acid linkage isomers on glycopeptides by ion mobility-mass spectrometry. *Chem. Commun.* **2016**; *52*: 4381-4384.

[16] Gray CJ, Thomas B, Upton R, Migas LG, Eyers CE, Barran PE, Flitsch SL. Applications of ionmobility mass spectrometry for high throughput, high resolution glycan analysis. *Biochim. Biophys. Acta* **2016**; *1860*: 1688-1709.

[17] Fenn LS, McLean JA. Simultaneous glycoproteomics on the basis of structure using ion mobility-mass spectrometry. *Mol. Biosyst.* **2009**; *5*: 1298-1302.

[18] Fenn LS, McLean JA. Structural separations by ion mobility-MS for glycomics and glycoproteomics. *Methods Molec. Biol.* **2013**; *951*: 171-194.

[19] Williams JP, Grabenauer M, Carpenter CJ, Holland RJ, Wormald MR, Giles K, Harvey DJ, Bateman RH, Scrivens JH, Bowers MT. Characterization of simple isomeric oligosaccharides and the rapid separation of glycan mixtures by ion mobility mass spectrometry. *Int. J. Mass Spectrom.* **2010**; *298*: 119–127.

[20] Plasencia MD, Isailovic D, Merenbloom SI, Mechref Y, Clemmer DE. Resolving and assigning *N*-linked glycan structural isomers from ovalbumin by IMS-MS. *J. Am. Soc. Mass Spectrom.* **2008**; *19*: 1706-1715.

[21] Jiao J, Zhang H, Reinhold VN. High performance IT-MS^n sequencing of glycans (spatial resolution of ovalbumin isomers). *Int. J. Mass Spectrom.* **2011**; *303*: 109-117.

[22] Isailovic D, Kurulugama RT, Plasencia MD, Stokes ST, Kyselova Z, Goldman R, Mechref Y, Novotny MV, Clemmer DE. Profiling of human serum glycans associated with liver cancer and cirrhosis by IMS-MS. *J. Proteome Res.* **2008**; *7*: 1109-1117.

[23] Harvey DJ, Scrivens JH, Holland R, Williams JP, Wormald MR. Ion-mobility separation coupled with negative ion fragmentation of *N*-linked carbohydrates. *Paper presented at the 56th ASMS Conference on Mass Spectrometry, Denver,* **2008**: Proceedings CD MOG 09.10.

[24] Hermannová M, Iordache A-M, Slováková K, Havlíček V, Pelantová H, Lemr K. Arrival time distributions of product ions reveal isomeric ratio of deprotonated molecules in ion mobility–mass spectrometry of hyaluronan-derived oligosaccharides. *J. Mass Spectrom.* **2015**; *50*: 854–863.

[25] Harvey DJ, Abrahams JL. Fragmentation and ion mobility properties of negative ions from N-linked carbohydrates: Part 7: Reduced glycans. *Rapid Commun. Mass Spectrom.* **2016**; *30*: 627-634.

[26] Harvey DJ, Sobott F, Crispin M, Wrobel A, Bonomelli C, Vasiljevic S, Scanlan CN, Scarff C, Thalassinos K, Scrivens JH. Ion mobility mass spectrometry for extracting spectra of *N*-glycans directly from incubation mixtures following glycan release: Application to glycans from engineered glycoforms of intact, folded HIV gp120. *J. Am. Soc. Mass Spectrom.* **2011**; *22*: 568-581.

[27] Harvey DJ, Crispin M, Bonomelli C, Scrivens JH. Ion mobility mass spectrometry for ion recovery and clean-up of MS and MS/MS spectra obtained from low abundance viral samples. *J. Am. Soc. Mass Spectrom.* **2015**; *26*: 1754-1767.

[28] Fenn LS, McLean JA. Biomolecular structural separations by ion mobility–mass spectrometry. *Anal. Bioanal. Chem.* **2008**; *391*: 905-909.

[29] Fenn LS, McLean JA. Enhanced carbohydrate structural selectivity in ion mobility-mass spectrometry analyses by boronic acid derivatization. *Chem. Commun.* **2008**: 5505-5507.

[30] Fenn LS, Kliman M, Mahsut A, Zhao SR, McLean JA. Characterizing ion mobility-mass spectrometry conformation space for the analysis of complex biological samples. *Anal. Bioanal. Chem.* **2009**; *394*: 235-244.

[31] Li H, Bendiak B, Siems WF, Gang DR, Hill Jr. HH. Ion mobility-mass correlation trend line separation of glycoprotein digests without deglycosylation. *Int. J. Ion Mobil. Spectrom.* **2013**; *16*: 105-115.

[32] Harvey DJ, Scarff CA, Edgeworth M, Crispin M, Scanlan CN, Sobott F, Allman S, Baruah K, Pritchard L, Scrivens JH. Travelling wave ion mobility and negative ion fragmentation for the structural determination of N-linked glycans. *Electrophoresis* **2013**; *34*: 2368-2378.

[33] Patel T, Bruce J, Merry A, Bigge C, Wormald M, Jaques A, Parekh R. Use of hydrazine to release in intact and unreduced form both N- and O-linked oligosaccharides from glycoproteins. *Biochemistry* **1993**; *32*: 679-693.

[34] Wing DR, Field MC, Schmitz B, Thor G, Dwek RA, Schachner MS, Rademacher TW. The use of large-scale hydrazinolysis in the preparation of N-linked oligosaccharide libraries: application to brain tissue. *Glycoconj. J.* **1992**; *9*: 293-301.

[35] de Waard P, Koorevaar A, Kamerling JP, Vliegenthart JFG. Structure determination by ^{1}H NMR spectroscopy of (sulfated) sialylated *N*-linked carbohydrate chains released from porcine thyroglobulin by peptide-N^4-(*N*-acetyl-β-glucosaminyl)asparagine amidase-F. *J. Biol. Chem.* **1991**; *266*: 4237-4243.

[36] Kamerling JP, Rijkse I, Maas AAM, van Kuik JA, Vliegenthart JFG. Sulfated *N*-linked carbohydrate chains in porcine thyroglobulin. *FEBS Letts.* **1988**; *241*: 246-250.

[37] Da Silva MLC, Stubbs HJ, Tamura T, Rice KG. ^{1}H-NMR characterization of a hen ovalbumin tyrosinamide N-linked oligosaccharide library. *Arch. Biochem. Biophys.* **1995**; *318*: 465-475.

[38] Harvey DJ, Wing DR, Küster B, Wilson IBH. Composition of N-linked carbohydrates from ovalbumin and co-purified glycoproteins. *J. Am. Soc. Mass Spectrom.* **2000**; *11*: 564-571.

[39] Yang Y, Barendregt A, Kamerling JP, Heck AJR. Analyzing protein micro-heterogeneity in chicken ovalbumin by high-resolution native mass spectrometry exposes qualitatively and semi-quantitatively 59 proteoforms. *Anal. Chem.* **2013**; *85*: 12037-12045.

[40] Green ED, Adelt G, Baenziger JU, Wilson S, van Halbeek H. The asparagine-linked oligosaccharides on bovine fetuin. Structural analysis of N-glycanase-released oligosaccharides by 500- Megahertz 1H-NMR spectroscopy. *J. Biol. Chem.* **1988**; *263*: 18253-18268.

[41] Fournet B, Montreuil J, Strecker G, Dorland L, Haverkamp J, Vliegenthart JFG, Binette JP, Schmid K. Determination of the primary structures of 16 asialo-carbohydrate units derived from human plasma α1-acid glycoprotein by 360 MHz ^{1}H NMR spectroscopy and permethylation analysis. *Biochemistry* **1978**; *17*: 5206-5214.

[42] Küster B, Hunter AP, Wheeler SF, Dwek RA, Harvey DJ. Structural determination of N-linked carbohydrates by matrix-assisted laser desorption/ionization mass spectrometry following

enzymatic release within sodium dodecyl sulfate-polyacrylamide electrophoresis gels: application to species-specific glycosylation of α1-acid glycoprotein. *Electrophoresis* **1998**; *19*: 1950-1959.

[43] Küster B, Wheeler SF, Hunter AP, Dwek RA, Harvey DJ. Sequencing of *N*-linked oligosaccharides directly from protein gels: In-gel deglycosylation followed by matrix-assisted laser desorption/ionization mass spectrometry and normal-phase high performance liquid chromatography. *Anal. Biochem.* **1997**; *250*: 82-101.

[44] Börnsen KO, Mohr MD, Widmer HM. Ion exchange and purification of carbohydrates on a Nafion$^{(R)}$ membrane as a new sample pretreatment for matrix-assisted laser desorption-ionization mass spectrometry. *Rapid Commun. Mass Spectrom.* **1995**; *9*: 1031-1034.

[45] Giles K, Pringle SD, Worthington KR, Little D, Wildgoose JL, Bateman RH. Applications of a travelling wave-based radio-frequency-only stacked ring ion guide. *Rapid Commun. Mass Spectrom.* **2004**; *18*: 2401-2414.

[46] Hernández H, Robinson CV. Determining the stoichiometry and interactions of macromolecular assemblies from mass spectrometry. *Nat. Protocols* **2007**; *2*: 715 - 726.

[47] Domon B, Costello CE. A systematic nomenclature for carbohydrate fragmentations in FAB-MS/MS spectra of glycoconjugates. *Glycoconj. J.* **1988**; *5*: 397-409.

[48] Harvey DJ. Electrospray mass spectrometry and collision-induced fragmentation of 2-aminobenzamide-labelled neutral N-linked glycans. *The Analyst* **2000**; *125*: 609-617.

[49] Pringle SD, Giles K, Wildgoose JL, Williams JP, Slade SE, Thalassinos K, Bateman RH, Bowers MT, Scrivens JH. An investigation of the mobility separation of some peptide and protein ions using a new hybrid quadrupole/travelling wave IMS/oa-ToF instrument. *Int. J. Mass Spectrom.* **2007**; *261*: 1-12.

[50] Bush MF, Hall Z, Giles K, Hoyes J, Robinson CV, Ruotolo BT. Collision cross sections of proteins and their complexes: A calibration framework and database for gas-phase structural biology. *Anal. Chem.* **2010**; *82*: 9557-9565.

[51] Pagel K, Natan E, Hall Z, Fersht AR, Robinson CV. Intrinsically disordered p53 and its complexes populate compact conformations in the gas phase. *Angew. Chem. Int. Ed.* **2013**; *52*: 361-365.

[52] Pagel K, Harvey DJ. Ion mobility mass spectrometry of complex carbohydrates - collision cross sections of sodiated *N*-linked glycans. *Anal. Chem.* **2013**; *85*: 5138-5145.

[53] Hofmann J, Struwe WB, Scarff CA, Scrivens JH, Harvey DJ, Pagel K. Estimating collision cross sections of negatively charged *N*-glycans using travelling wave ion mobility-mass spectrometry. *Anal. Chem.* **2014**; *86*: 10789-10795.

[54] Thalassinos K, Grabenauer M, Slade SE, Hilton GR, Bowers MT, Scrivens JH. Characterization of phosphorylated peptides using traveling wave-based and drift cell ion mobility mass spectrometry. *Anal. Chem.* **2009**; *81*: 248-254.

[55] May JC, Goodwin CR, Lareau NM, Leaptrot KL, Morris CB, Kurulugama RT, Mordehai A, Klein C, Barry W, Darland E, Overney G, Imatani K, Stafford GC, Fjeldsted JC, McLean JA. Conformational ordering of biomolecules in the gas phase: Nitrogen collision cross sections measured on a prototype high resolution drift tube ion mobility-mass spectrometer. *Anal. Chem.* **2014**; *86*: 2107-2116.

[56] Campbell MP, Struwe W, Pagel K, Benesch JLP, Harvey DJ. GlycoMob - an ion mobility mass spectrometry database. *Glycobiology* **2015**; *25*: 1275-1276.

[57] Li H, Bendiak B, Siems WF, Gang DR, Hill J, Herbert H. Ion mobility mass spectrometry analysis of isomeric disaccharide precursor, product and cluster ions. *Rapid Commun. Mass Spectrom.* **2013**; *27*: 2699–2709.

[58] Gaye MM, Kurulugama R, Clemmer DE. Investigating carbohydrate isomers by IMS-CID-IMS-MS: Precursor and fragment ion cross-sections. *Analyst* **2015**; *140*: 6922-6932.

[59] Harvey DJ, Scarff CA, Crispin M, Scanlan CN, Bonomelli C, Scrivens JH. MALDI-MS/MS with traveling wave ion mobility for the structural analysis of *N*-linked glycans. *J. Am. Soc. Mass Spectrom.* **2012**; *23*: 1955-1966.

[60] Saba J, Zumwalt A, Meitei NS, Apte A, Viner R. Automated glycan structural isomer differentiation using a bioinformatics tool. *Proceedings of the 59th ASMS Conference on Mass Spectrometry and Allied Topics, Denver* **2011**: TP08 170.

[61] Harvey DJ, Edgeworth M, Krishna BA, Bonomelli C, Allman S, Crispin M, Scrivens JH. Fragmentation of negative ions from *N*-linked carbohydrates: Part 6: Glycans containing one N-acetylglucosamine in the core. *Rapid Commun. Mass Spectrom.* **2014**; *28*: 2008–2018.

[62] Harvey DJ, Crispin M, Scanlan C, Singer BB, Lucka L, Chang VT, Radcliffe CM, Thobhani S, Yuen C-T, Rudd PM. Differentiation between isomeric triantennary *N*-linked glycans by negative ion tandem mass spectrometry and confirmation of glycans containing galactose

attached to the bisecting (β1-4-GlcNAc) residue in *N*-glycans from IgG. *Rapid Commun. Mass Spectrom.* **2008**; *22*: 1047-1052.
[63] Gabryelski W, Froese KL. Rapid and sensitive differentiation of anomers, linkage, and position isomers of disaccharides using High-Field Asymmetric Waveform Ion Mobility Spectrometry (FAIMS). *J. Am. Soc. Mass Spectrom.* **2003**; *14*: 265-277.
[64] Hernandez O, Isenberg S, Steinmetz V, Glish GL, Maitre P. Probing mobility-selected saccharide isomers: Selective ion-molecule reactions and wavelength-specific IR activation. *J. Phys. Chem. A* **2015**; *119*: 6057-6064.
[65] Clowers BH, Dwivedi P, Steiner WE, Hill HHJ, Bendiak B. Separation of sodiated isobaric disaccharides and trisaccharides using electrospray ionization-atmospheric pressure ion mobility-time of flight mass spectrometry. *J. Am. Soc. Mass Spectrom.* **2005**; *16*: 660-669.
[66] Li H, Giles K, Bendiak B, Kaplan K, Siems WF, Hill HH, Jr. Resolving structural isomers of monosaccharide methyl glycosides using drift tube and traveling wave ion mobility mass spectrometry. *Anal. Chem.* **2012**; *84*: 3231-3239.
[67] Both P, Green AP, Gray CJ, Šardzík R, Voglmeir J, Fontana C, Austeri M, Rejzek M, Richardson D, Field RA, Widmalm G, Flitsch SL, Eyers CE. Discrimination of epimeric glycans and glycopeptides using IM-MS and its potential for carbohydrate sequencing. *Nat. Chem.* **2014**; *6*: 65-74.
[68] Dwivedi P, Bendiak B, Clowers BH, Hill HHJ. Rapid resolution of carbohydrate isomers by electrospray ionization ambient pressure ion mobility spectrometry-time-of-flight mass spectrometry (ESI-APIMS-TOFMS). *J. Am. Soc. Mass Spectrom.* **2007**; *18*: 1163-1175.
[69] Harvey DJ, Merry AH, Royle L, Campbell MP, Dwek RA, Rudd PM. Proposal for a standard system for drawing structural diagrams of *N*- and *O*-linked carbohydrates and related compounds. *Proteomics* **2009**; *9*: 3796-3801.

Table 1, Estimated collisional cross sections of hybrid and complex glycans

(Major isomers of high-mannose glycans included for comparison)

Compound	Structure[a]	*m/z*[b]	Source	Instrument[c]	Cal.[d]	Cross section			
						Nitrogen			He[e]
						Å^2	SD	n	Å^2
H_3N_2	**45**	1007.3	Ovalbumin	G2Si	I	284.6	0.16	12	206.6
H_3N_3	**5**	1210.4	Ovalbumin	G2Si	I	310.0	0.20	9	229.4
H_3N_3	**6**	1210.4	Ovalbumin	G2Si	I	322.1	0.19	9	240.4
H_5N_2	**1**	1331.4	Ovalbumin	G2Si	I	339.0	0.18	12	256.1
H_4N_3	**4**	1372.5	Ovalbumin	G2Si	I	336.0[f]	0.36	12	253.4
H_3N_4	**7**	1413.5	Ovalbumin	G2Si	I	347.7	0.19	12	262.6
H_6N_2	**46**	1493.5	Ovalbumin	G2Si	I	364.1	0.22	12	277.8
H_5N_3	**2**	1534.5	gp120	G2Si	E	373.9	-	-	287.5
H_5N_3	**47**	1534.5	gp120	G2Si	E	357.6	-	-	272.2
$H_3N_4F_1$	**13**	1559.5	IgG	G2Si	I	377.9	1.00	6	290.5
H_4N_4	**8,9**	1575.5	Ovalbumin	G2Si	I	365.3	0.49	12	278.8
H_3N_5	**37**	1616.5	IgG	G2Si	E	378.8	1.36	5	291.2
			Ovalbumin	G2Si	I	382.4	0.30	12	294.2
H_7N_2	**53**	1655.5	Thyroglobulin	G2Si	I	387.9	0.53	12	299.2
$H_5N_3F_1$	**48**	1680.5	gp120	G2	E	389.4	-	1	300.9
				G2Si	E	385.4	-	1	296.9
$H_5N_3F_1$	**49**	1680.5	gp120	G2Si	E	405.0	-	1	314.5
H_6N_3	**3**	1696.6	Ovalbumin	G2Si	I	381.0	0.61	12	293.1
$H_4N_4F_1$	**14,15**	1721.6	IgG	G2	E	399.0	1.2	4	309.5
			Thyroglobulin	G2Si	I	398.8	0.78	3	308.6
$H_4N_4F_1$	**14,15**	1721.6	Thyroglobulin	G2Si	I	397.5	0.65	19	308.2
H_5N_4	**10**	1737.6	IgG,	G2	E	392.0	0.29	9	303.2
			Fetuin	G2	E	388.4	1.30	5	299.5
			AGP	G2Si	E	392.4	0.57	2	303.5
H_5N_4	**25**	1737.6	Ovalbumin	G2Si	I	393.5	0.28	12	304.8
$H_3N_5F_1$	**41**	1762.6	IgG	G2	E	407.3	0.17	4	316.8
			IgG	G2Si	E	403.8	1.49	5	313.2
H_4N_5	**29,30,40**	1778.6	Ovalbumin	G2Si	I	401.5	0.33	12	311.9
H_8N_2	**53**	1817.6	Thyroglobulin	G2Si	I	418.5[f]	2.28	12	327.0
H_3N_6	**27,28**	H_3N_6	Ovalbumin	G2Si	I	411.4[g]	0.30	12	321.2
$H_5N_4F_1$	**16**	1883.6	Thyroglobulin	G2Si	I	418.8	0.96	19	327.3
			AGP	G2Si	E	418.0	0.28		326.6
$H_4N_5F_1$	**42,43**	1924.6	IgG	G2Si	E	420.4	0.21	5	328.5
H_5N_5	**40**	1940.6	IgG	G2Si	E	421.6	-	-	329.3
	29,30		Ovalbumin	G2Si	I	420.6[h]	0.58	12	330.3
H_9N_2	**54**	1979.6	Thyroglobulin	G2Si	I	434.1[f]	1.34	12	342.0
H_4N_6	**31,32**[i]	1981.7	Ovalbumin	G2Si	I	427.6	0.56	12	335.5
H_3N_7	**33**	2022.7	Ovalbumin	G2Si	I	434.5	0.66	12	341.3
$H_5N_5F_1$	**44**	2086.7	IgG	G2	E	443.9	0.30	4	349.2
				G2Si	E	439.4	0.95	4	345.7
H_6N_5	**19**	2102.7	AGP	G2Si	E	441.8	0.78	2	348.8
H_4N_7	**35**	2184.7	Ovalbumin	G2Si	I	453.1	0.90	12	359.0
H_3N_8	**34**	2225.8	Ovalbumin	G2Si	I	462.0	0.55	12	366.4
$H_6N_5F_1$	**17**	2248.7	AGP	G2Si	E	464.5	0.35	2	368.8
H_7N_6	**22**	2467.8	AGP	G2Si	E	484.9	0.00	2	-
$H_7N_6F_1$	**21**	2613.9	AGP	G2Si	E	510.4	0.42	2	-

a) Structures are in Scheme 1.
b) $[M+H_2PO_4]^-$ ion.
c) Measurements with the G2 instrument were averages of those made at various times over three years.
d) I = Internal calibration. E = External calibration; these were made on the same day and are the mean values obtained by varying the gas flow, wave velocity and wave height.
e) Estimated from helium/nitrogen correlation plot.
f) Asymmetric peak
g) Major isomer (minor isomer too low in abundance to give an accurate cross section measurement).
h) Isomers detected by fragment ion plots.
i) Isomers not resolved.

Legends for figures and schemes

Scheme 1. Structures of the *N*-glycans discussed in the text. Symbols for the glycan constituents and linkages between them are: ■ = GlcNAc, ● = mannose, ◆ = galactose, ◆ = fucose. Solid connecting line = β-linkage, broken line = α-linkage. The angle of the lines shows the linkage position:

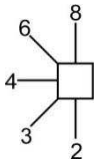

For more information see[69]. Compositions are given by H = hexose, N = GlcNAc, F = fucose. Monoisotopic masses listed below the compositions are of the $[M+H_2PO_4]^-$ ions.

Figure 1. Negative ion ESI spectra of *N*-glycans released from (**a**) chicken ovalbumin, (**b**) porcine thyroglobulin, (**c**) human IgG, (**d**), gp120 and (**e**) α1-acid glycoprotein (AGP). Symbols for the structures shown in this and the other figures are as defined in the legend to Scheme 1 with the addition of ★ = Neu5Ac (sialic acid). Numbers in bold accompanying the structures are listed in Scheme 1.

Figure 2. (**a**) Plot of CCS against *m/z* for the phosphate adducts of the *N*-glycans. Numbers refer to the structures listed in Scheme 1. (**b**) A similar plot of the phosphate adducts of the reduced glycans. (**c**) Plot of cross section against *m/z* for the sodium adducts of the *N*-glycans (positive ion mode. (**d**) Corresponding plot of the sodium adducts of the reduced glycans. Black circles, biantennary glycans; red circles, high-mannose glycans; inverted green triangles, $Man_3GlcNAc_{2\text{-}8}$ series; yellow triangles, remainder of ovalbumin glycans; blue squares, tetra-antennary glycans; pink squares, triantennary glycans.

Figure 3. Plot of estimated nitrogen CCSs against *m/z* for the phosphate adducts of biantennary glycans from IgG with zero, one and two galactose residues. The four lines connect these glycans having additional core fucose (**13**-**16**, red circles), bisecting GlcNAc (**37-40**, green inverted triangles), both fucose and bisecting GlcNAc (**41-44**, yellow triangles) and no additional substituents (**7-10**, black circles). Error are standard deviations (n = 5).

Figure 4. (**a**) ATD plot of *m/z* 1136 ($Man_3GlcNAc_3$, **5**, **6**, $M+Na]^+$ ion) from chicken ovalbumin recorded with the Synapt G2 instrument (wave velocity 600 m/sec, wave height 40 V) showing separation of isomers. (**b**) Corresponding negative ion plot ($[M+H_2PO_4]^-$ ions, wave velocity 450, wave height 40 V), (**c** and **d**) Positive ion CID spectra of the compounds producing the two peaks in the ATD profile shown in panel **a**. (**e** and **f**) Negative ion CID spectra of the compounds producing the two peaks in the ATD profile shown in panel **b**. Fragment ions are labelled according to the scheme proposed by Domon and Costello[47].

Figure 5. (**a**) Negative ion CID spectrum of the ion at *m/z* 1321 from the nitrate adducts of *N*-glycans released from porcine thyroglobulin (G1 instrument, wave velocity 450 m/sec, wave height 14 V) (**b**) ion mobility profile of *m/z* 1321 showing separation of singly and doubly charged ions (**c**) extracted fragment ATDs from the singly charged ion at *m/z* 1321 obtained in the transfer cell (**d**) CID spectrum from the leading edge of the mobility peak (compound **11**) (**e**) CID spectrum from the trailing edge of the mobility peak (compound **12**).

Figure 6. (**a**) Negative ion CID spectrum of the hybrid *N*-glycan $Gal_1Man_5GlcNAc_3Fuc_1$ (**50**, *m/z* 1842.6). (**b**) Negative ion CID spectrum of the hybrid *N*-glycan $Gal_1Man_4GlcNAc_3Fuc_1$ (**48**, *m/z* 1680.5). (**c**) Negative ion CID spectrum of the hybrid *N*-glycan $Man_5GlcNAc_3Fuc_1$ (**49**, *m/z* 1680.5). The inset shows extracted fragment ATDs of diagnostic fragment ions from the spectra shown in panels **b** and **c**. (**a**) Negative ion CID spectrum of the hybrid *N*-glycan $Man_4GlcNAc_3$ (**4**, *m/z* 1372.4).

Figure 7. (**a**) ATD profiles of the $[M+H_2PO_4]^-$ ions from the isomeric biantennary (**10**) and hybrid (**25**) glycans of composition $Hex_5GlcNAc_4$ (*m/z* 1737). Both peaks have been normalized to 100%. (**b**)

Extracted fragment ATDs of diagnostic fragment ions for the peak at *m/z* 1737.6 from chicken ovalbumin. The spectrum is shown in panel **c**. Most ions arise from the bisected hybrid glycan (**25**). (**d**) Negative ion CID spectrum of the biantennary complex glycan $Man_5GlcNAc_4$ (**10**, *m/z* 1737.6). The ion at *m/z* 424 characterizes the biantennary structure.

Figure 8. (**a**) ATDs of the D, D-18 and D-221 fragment ions from the $[M+H_2PO_4]^-$ ions of the monogalactosylated biantennary glycans (**8**, **9**) and bisected hybrid glycans ($Hex_4GlcNAc_4$, *m/z* 1575.5 from ovalbumin showing slight separation of the isomers. (**b**) Negative ion CID spectrum of the peak at *m/z* 1575.5 from chicken ovalbumin containing a mixture of the glycans **8**, **9** and **24**.

Figure 9. (**a**) ATDs of the D and D-18 fragment ions from the $[M+H_2PO_4]^-$ ions from the monogalactosylated biantennary glycans (**8**, **9**, *m/z* 1575.5) from IgG showing slight separation of the two isomers (**8**, **9**). (**b**) Corresponding plots from the core-fucosylated glycans (**14**, **15**) showing no separation. (**c**) Negative ion CID spectrum of the $[M+H_2PO_4]^-$ ions from the two fucosylated monogalactosylated biantennary glycans (**14**, **15**) from IgG with D and D-18 ions confirming the presence of the two isomers.

Figure 10. Negative ion CID spectrum of the mixture of the two triantennary glycans **17** and **18** ($Gal_3Man_3GlcNAc_5Fuc_1$, *m/z* 2248.8 from gp120 (JFRC). The isomer with the branched 3-antenna (**17**) is characterized by the ions at *m/z* 831 (E), 688 (D) and 670 (D-18) and the isomer with the branched 6-antenna (**18**) produces the ions at *m/z* 1053 (D), 1035 (D-18) and 1017 (D-36)[62]. The inset is of the ATD profiles of the ions at *m/z* 831 and 1035 showing slight separation.

Abbreviations

ATD, arrival time distribution; CCS, collisional cross section, CID, collision-induced decomposition; ESI, electrospray ionization; Fuc, fucose; G1, Waters Synapt ion mobility mass spectrometer, first generation; G2, Waters Synapt ion mobility mass spectrometer, second generation; G0, G1, G2, biantennary glycans with zero, one and two galactose residues respectively; G0F, G1F, G2F, Core fucosylated biantennary glycans with zero, one and two galactose residues respectively; Gal, galactose, Glc, glucose; GlcNAc, *N*-acetylglucosamine; HEK, human embryonic kidney; HPLC, high-performance liquid chromatography; Hex, hexose; IgG, immunoglobulin G; LC, liquid chromatography; Man, mannose; MS, mass spectrometry; Neu5Ac, *N*-acetylneuraminic acid (sialic acid); PAGE, polyacrylamide gel electrophoresis; PEG, polyethylene glycol; PNGase F, protein *N*-glycosidase F; TOF, time-of-flight; TWIMS, T-wave ion mobility spectrometry.

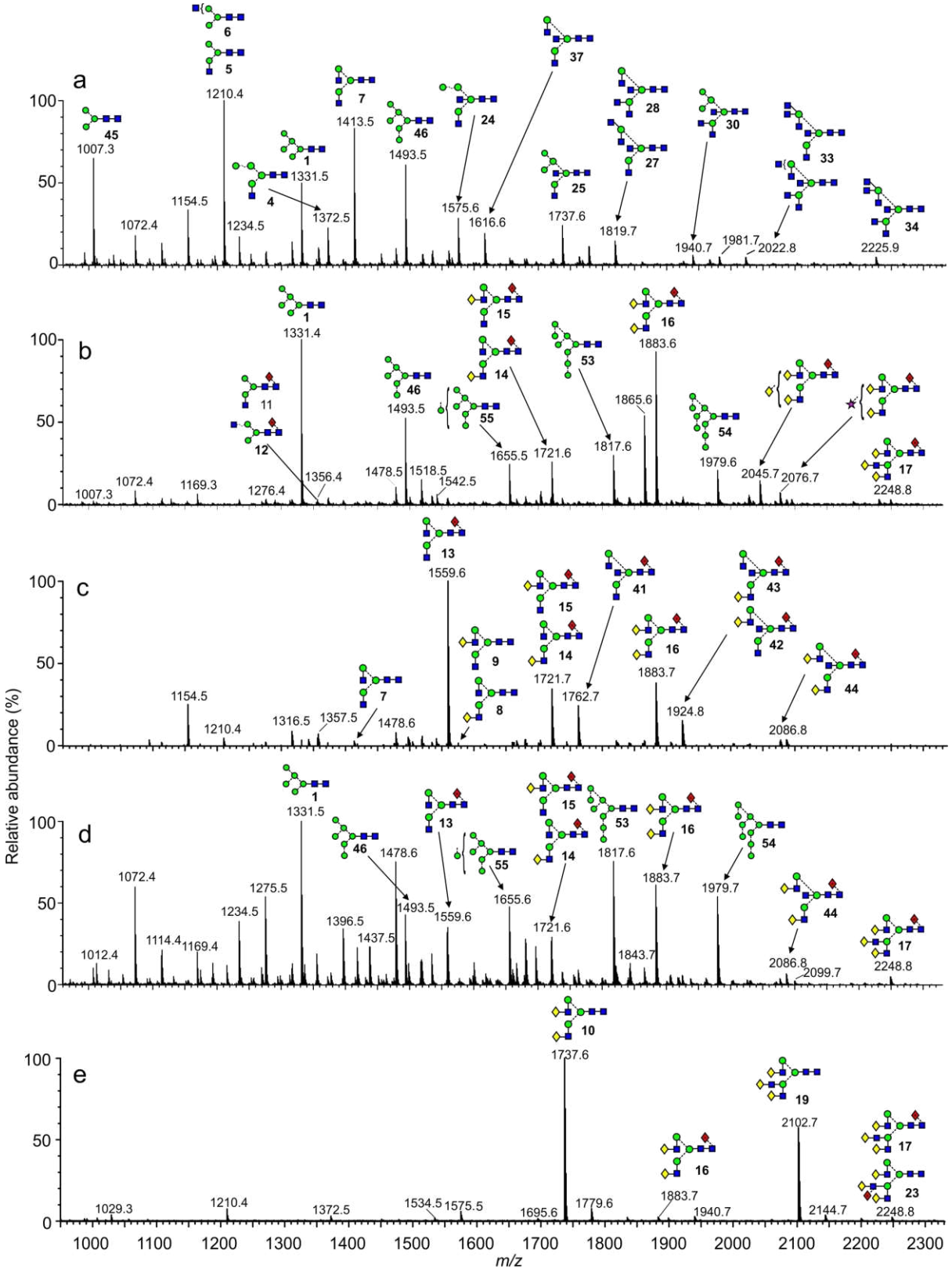
a
b
c
d
e
Relative abundance (%)
m/z
1000
1100
1200
1300
1400
1500
1600
1700
1800
1900
2000
2100
2200
2300

Figure 1

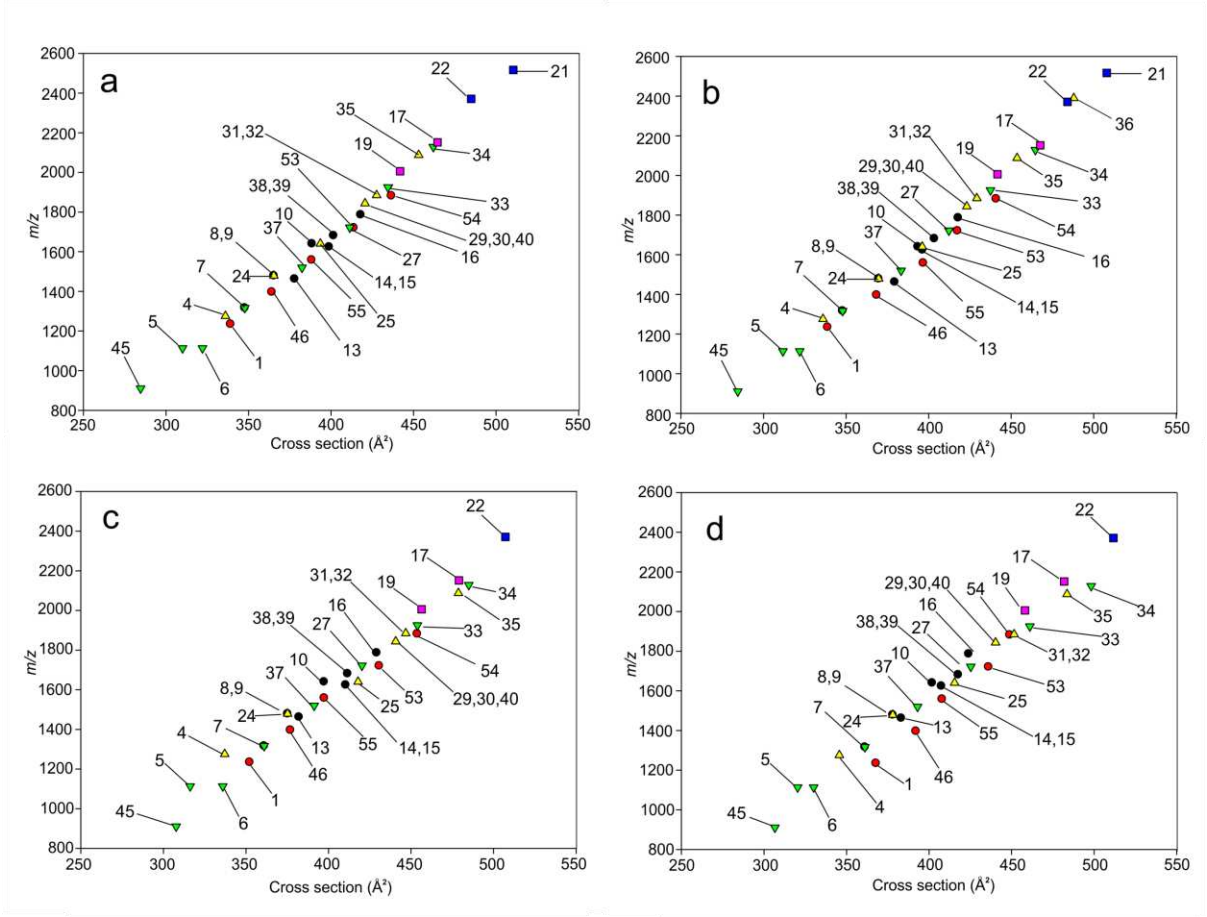

Figure 2

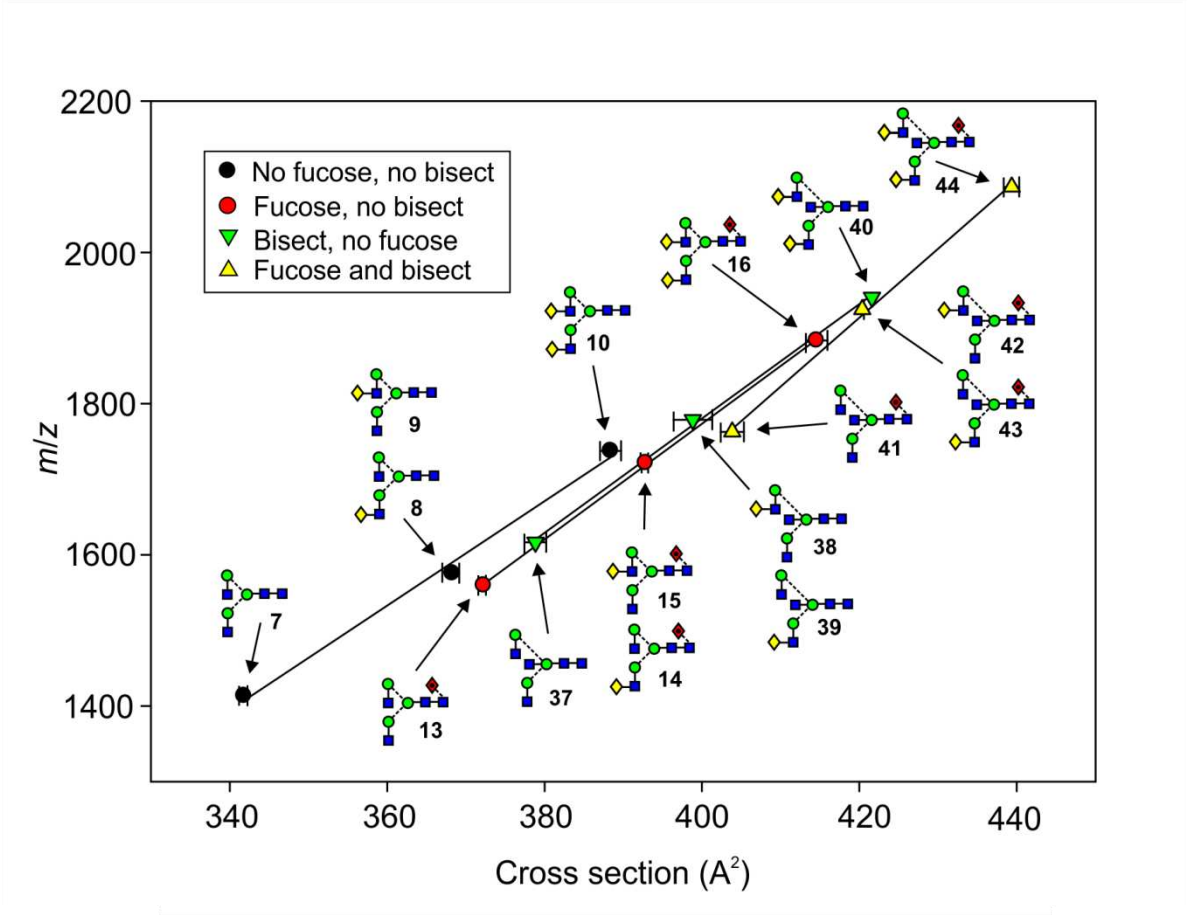
No fucose, no bisect
Fucose, no bisect
Bisect, no fucose
Fucose and bisect
m/z
Cross section (A²)
2200
2000
1800
1600
1400
340
360
380
400
420
440
7
8
9
10
13
14
15
16
37
38
39
40
41
42
43
44

Figure 3

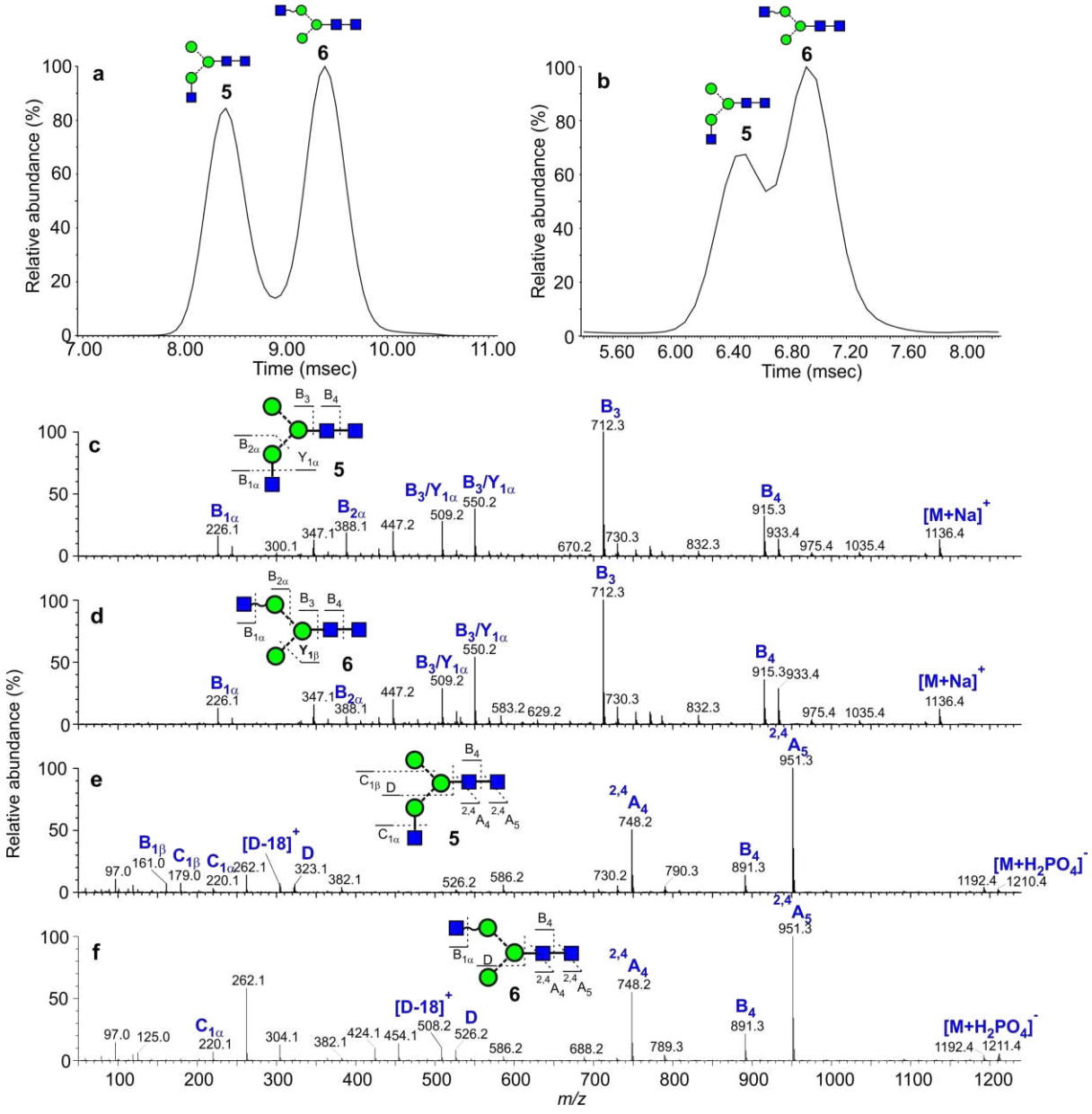
a
b
c
d
e
f
Relative abundance (%)
Time (msec)
m/z
5
6
B3
712.3
B4
915.3
[M+Na]+
1136.4
B1α
226.1
B2α
388.1
B3/Y1α
550.2
2,4A5
951.3
2,4A4
748.2
[D-18]+
D
C1α
220.1
C1β
179.0
B1β
161.0
[M+H2PO4]-
1192.4

Figure 4

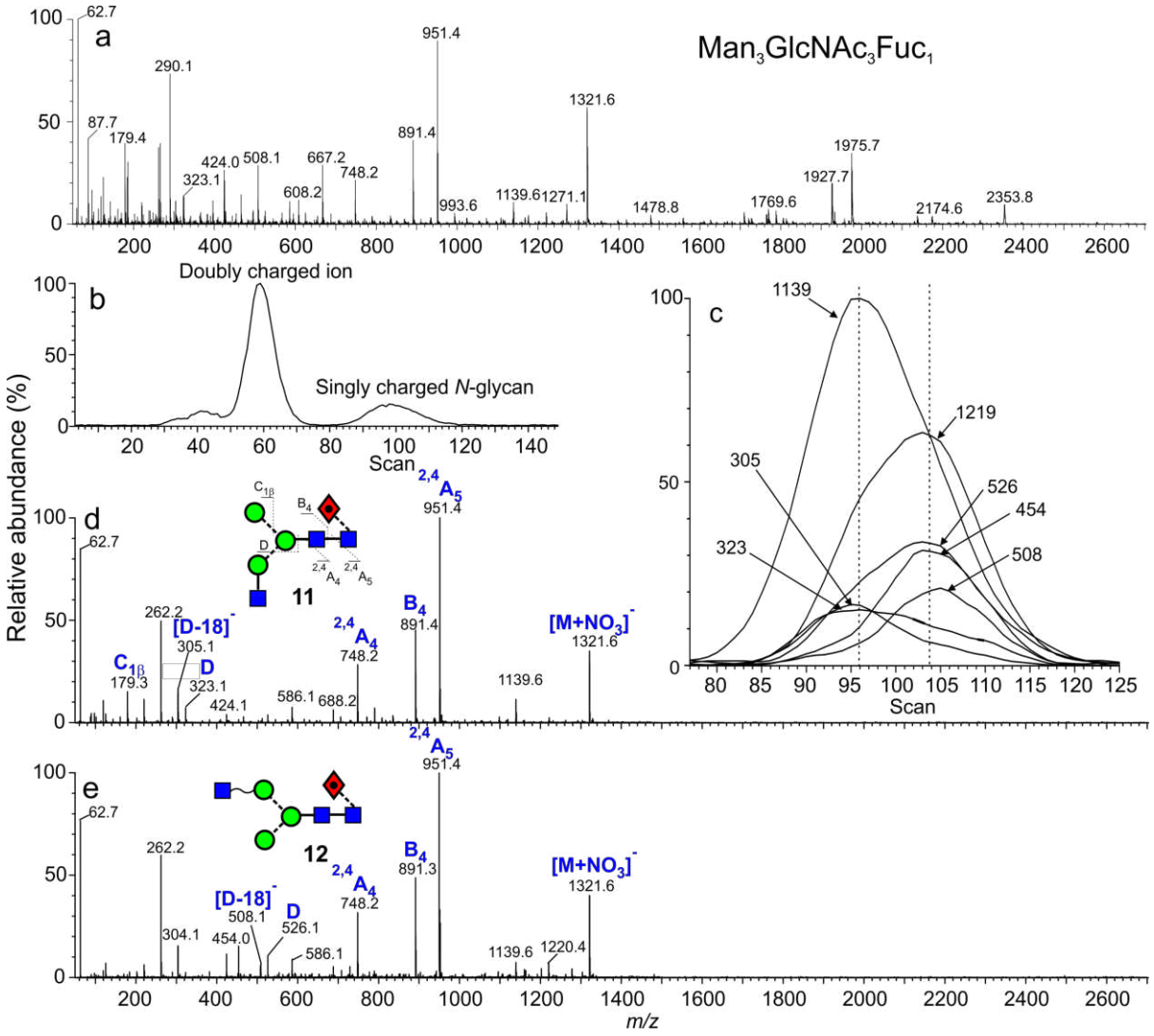
a
Man3GlcNAc3Fuc1
b
Doubly charged ion
Singly charged N-glycan
Scan
c
Scan
d
e
m/z
Relative abundance (%)
[D-18]-
[M+NO3]-
B4
C1β
D
11
12

Figure 5

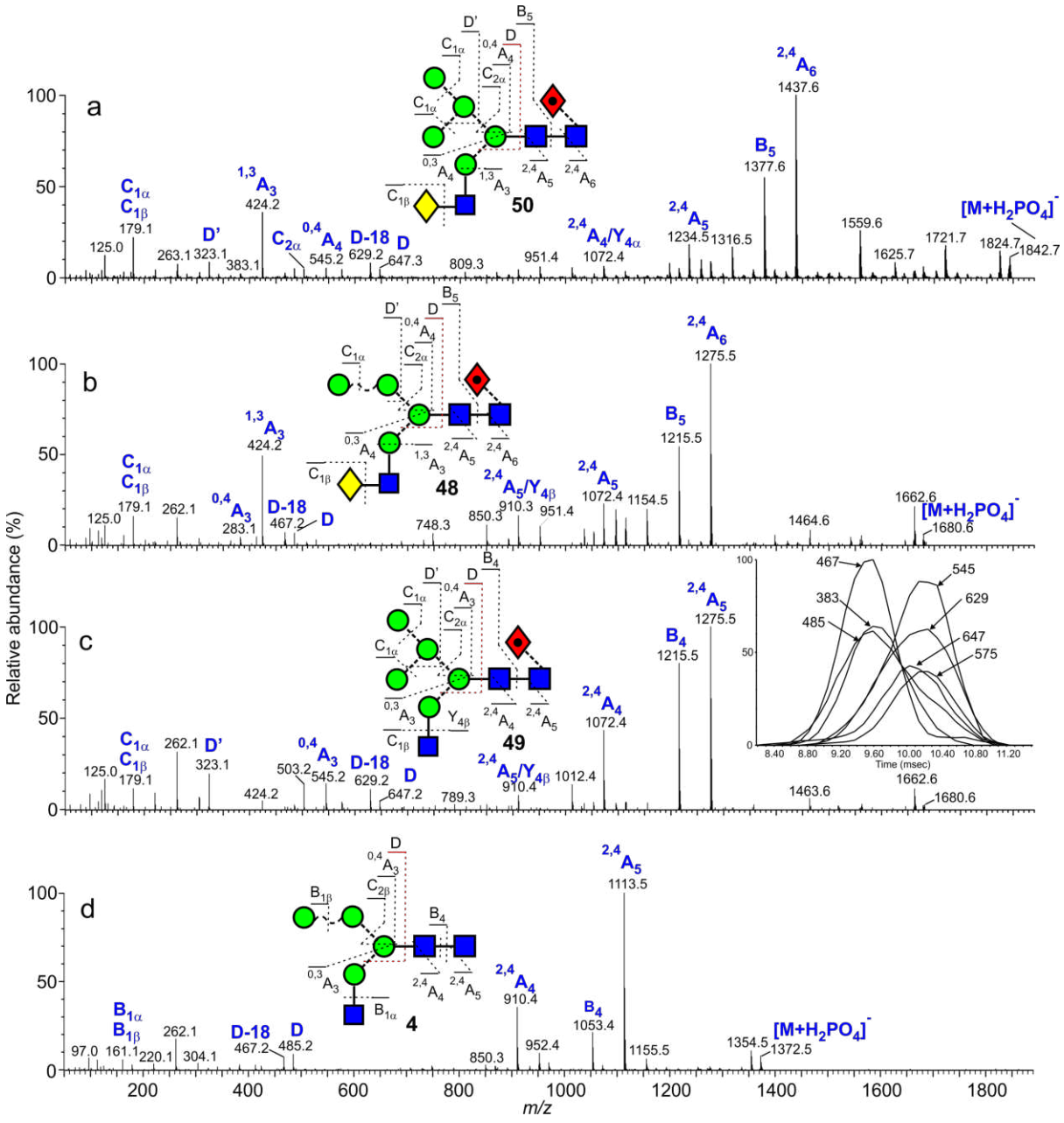

Figure 6

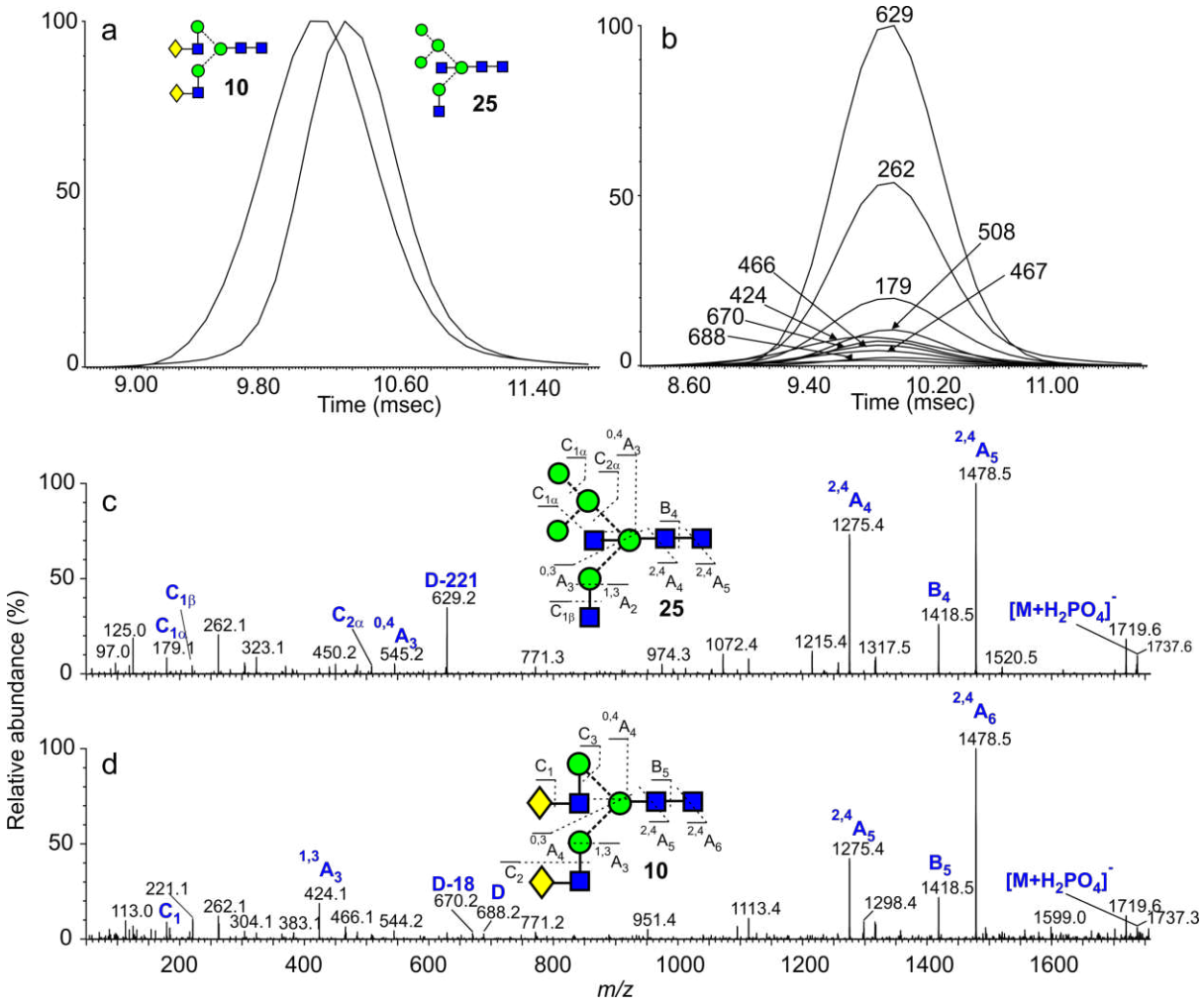
a
10
25
100
50
0
9.00
9.80
10.60
11.40
Time (msec)
b
629
262
508
466
467
424
179
670
688
100
50
0
8.60
9.40
10.20
11.00
Time (msec)
c
C1α
C2α
0,4A3
B4
0,3A3
2,4A4
2,4A5
1,3A2
C1β
25
C1β
C1α
D-221
629.2
2,4A4
1275.4
2,4A5
1478.5
B4
1418.5
[M+H2PO4]-
1719.6
1737.6
125.0
97.0
179.1
262.1
323.1
450.2
545.2
771.3
974.3
1072.4
1215.4
1317.5
1520.5
d
C3
0,4A4
C1
B5
0,3A4
2,4A5
2,4A6
1,3A3
C2
10
2,4A6
1478.5
2,4A5
1275.4
B5
1418.5
[M+H2PO4]-
1719.6
1737.3
1,3A3
424.1
D-18
670.2
D
688.2
221.1
113.0
C1
262.1
304.1
383.1
466.1
544.2
771.2
951.4
1113.4
1298.4
1599.0
Relative abundance (%)
200
400
600
800
1000
1200
1400
1600
m/z

Figure 7

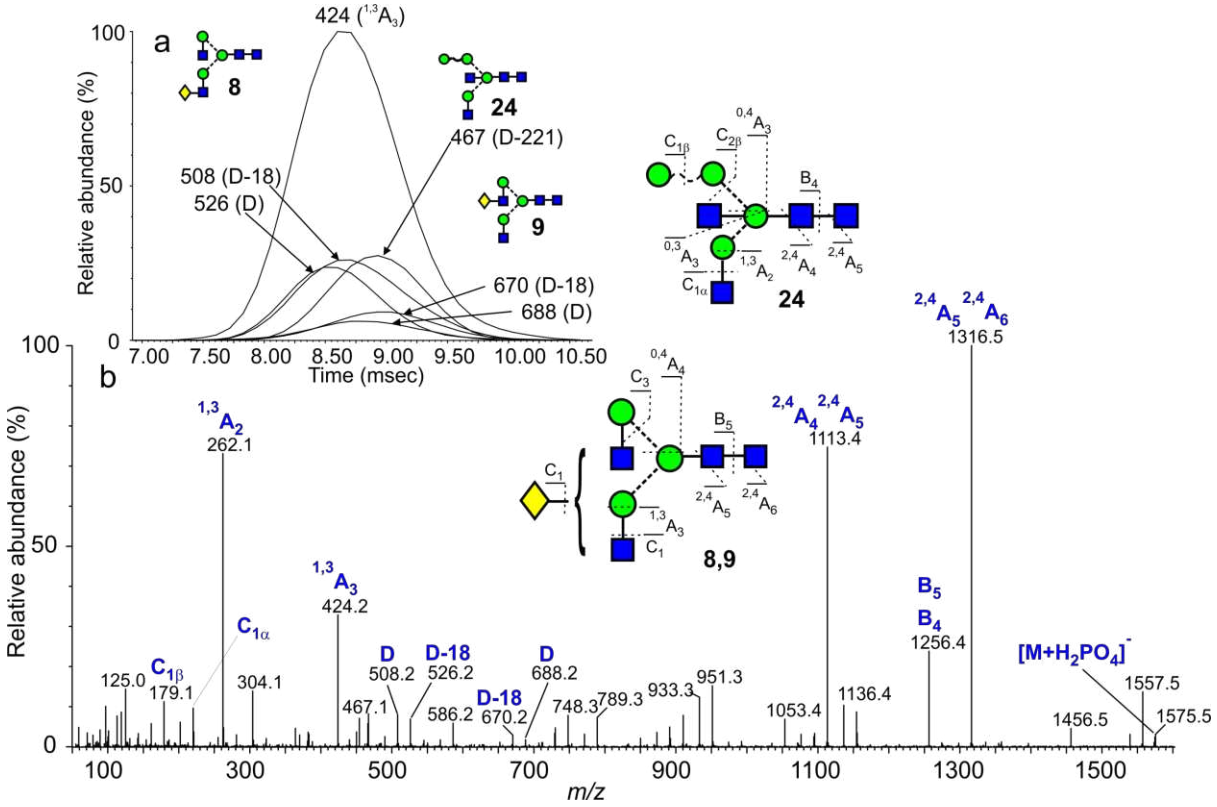
a
424 (1,3A3)
8
24
467 (D-221)
508 (D-18)
526 (D)
9
670 (D-18)
688 (D)
Relative abundance (%)
Time (msec)
b
1,3A2 262.1
1,3A3 424.2
C1α
C1β 179.1
125.0
304.1
D 508.2
D-18 526.2
467.1
586.2
D-18 670.2
D 688.2
748.3
789.3
933.3
951.3
1053.4
2,4A4 2,4A5 1113.4
1136.4
B5 B4 1256.4
2,4A5 2,4A6 1316.5
[M+H2PO4]-
1557.5
1456.5
1575.5
8,9
24
m/z

Figure 8

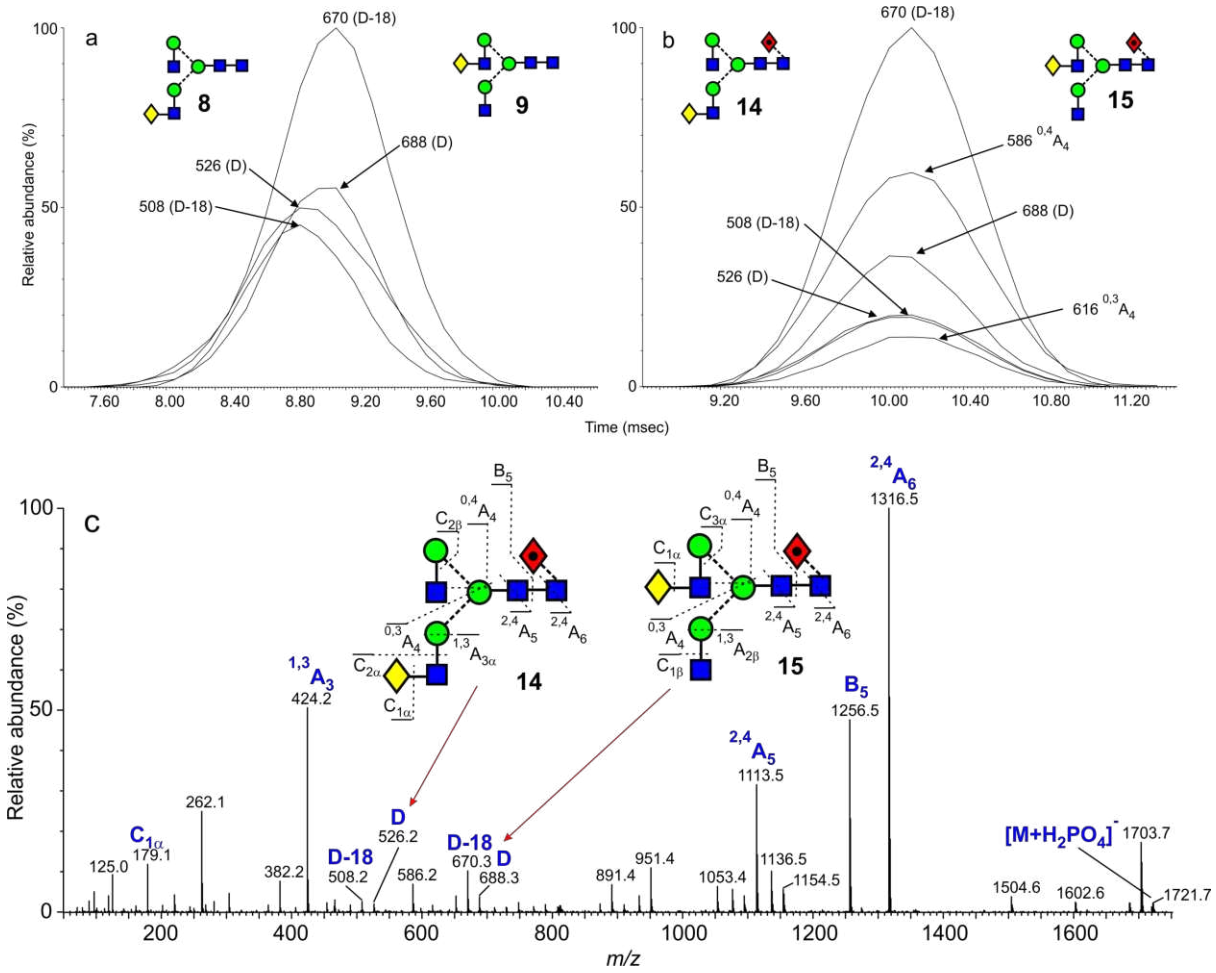
a
b
c
Relative abundance (%)
Time (msec)
m/z
670 (D-18)
688 (D)
526 (D)
508 (D-18)
586 0,4A4
616 0,3A4
8
9
14
15
1,3A3 424.2
2,4A6 1316.5
B5 1256.5
2,4A5 1113.5
C1α 179.1
D 526.2
D-18 508.2
D-18 670.3
D 688.3
[M+H2PO4]- 1703.7
262.1
125.0
382.2
586.2
891.4
951.4
1053.4
1136.5
1154.5
1504.6
1602.6
1721.7

Figure 9

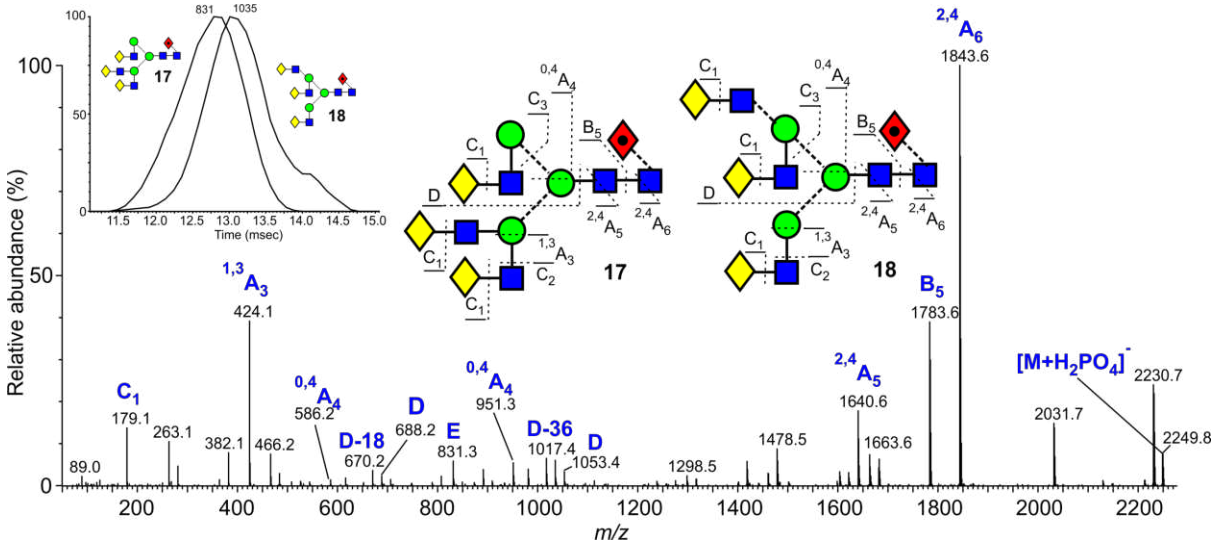
831
1035
17
18
Time (msec)
Relative abundance (%)
m/z
17
18
1,3 A3
424.1
C1
179.1
263.1
382.1
466.2
0,4 A4
586.2
D-18
670.2
D
688.2
E
831.3
0,4 A4
951.3
D-36
1017.4
D
1053.4
1298.5
1478.5
2,4 A5
1640.6
1663.6
B5
1783.6
2,4 A6
1843.6
2031.7
[M+H2PO4]-
2230.7
2249.8
89.0

Figure 10